Received: 19 October 2023 | Revised: 12 December 2023 | Accepted: 26 December 2023

DOI: 10.1002/eqe.4080

WILEY

RESEARCH ARTICLE

Seismic response and capacity of inelastic acceleration-sensitive nonstructural elements subjected to building floor motions

Gennaro Magliulo[1,2] | **Danilo D'Angela**[1]

[1]Department of Structures for Engineering and Architecture, University of Naples Federico II, Napoli, Italy

[2]Construction Technologies Institute (ITC), National Research Council (CNR), Napoli, Italy

Correspondence
Gennaro Magliulo, Department of Structures for Engineering and Architecture, University of Naples Federico II, Via Claudio 21, 80125 Napoli, Italy.
Email: gmagliul@unina.it

Funding information
Italian Ministry of University and Research; Italian Department of Civil Protection

Abstract

The paper investigates the seismic response of nonstructural elements (NEs), focusing on acceleration-sensitive components housed in buildings, modelled as inelastic Ibarra–Medina–Krawinkler (SDOF) systems. Incremental dynamic analysis (IDA) is carried out considering (a) representative suites of building floor motions (real loading histories recorded within reinforced concrete (RC) buildings and table testing protocol inputs) and (b) a wide range of NE models (with elastic frequencies ranging within 1–9 Hz). The Ibarra-Medina-Krawinkler (IMK) model was implemented in OpenSees, defining the key modeling parameters according to the formulations provided by Lignos and Krawinkler. Both IDA curves and component (acceleration) amplification factor (CAF) are characterized, also considering statistical measures. The seismic capacity of the investigated NEs is estimated through fragility curves, accounting for five incremental damage states (DSs). The fragility parameters are correlated with the frequency of the NE models, and (statistical-based) closed-form capacity criteria are provided. The study provides a robust technical and scientific methodological framework for assessing the seismic capacity of NEs that can be modeled by inelastic SDOF systems. The findings have a potential major impact on both research and practice, enriching scientific knowledge and providing useful applicative tools. In particular, quantitative response and capacity measures are supplied, and the developed capacity criteria can be particularly useful for expeditious but reliable design and assessment, as well as for comparison purposes.

KEYWORDS

floor motions, inelastic behavior, Nonstructural elements, seismic fragility, seismic performance

RESEARCH HIGHLIGHTS

- Seismic response and capacity assessment of inelastic acceleration-sensitive nonstructural elements housed in buildings.
- Characterization of the influence of floor motion type (real records and shake table protocol inputs).
- Evaluation of the effects of inelasticity on acceleration amplification and seismic capacity.
- Estimation of closed-form statistical-based capacity criteria and related uncertainties.

1 | INTRODUCTION

Advanced seismic safety assessment of nonstructural elements (NEs) is based on the comparison of capacity and demand measures, often statistically expressed in terms of engineering demand parameters (EDPs) for the relevant performance levels or limit states, based on the identification of the appropriate damage states (DSs) or damage criteria. The NE seismic safety assessment methodology is typically derived from the performance-based earthquake engineering (PBEE) approach developed for engineering structures.[1,2] These capacity and safety estimations are essential to mitigate seismic risk associated with NEs.[3–5] The focus of the present study is on the seismic assessment of seismic response and capacity of NEs, in the framework of PBEE.

The seismic capacity of NEs is often assessed through the implementation of statistical-based methods, and fragility curves represent the state-of-the-art.[6–8] Experimental assessment represents the most reliable method for estimation of the seismic capacities of NEs,[9–14] even though other methods might be more efficient and economic, still being relatively reliable. In the last few decades, the seismic capacity of NEs was also estimated by means of numerical or analytical approaches,[15–21] often experimentally calibrating the modeling and analysis parameters. In a few cases, observational data were used to assess the seismic response of NEs and to provide capacity thresholds.[22,23] Very recent studies assessed the seismic response and capacity of NEs modeled as inelastic systems by means of advanced numerical models.[24–27] Technical reports and guidelines provide quantitative tools to expeditiously estimate seismic capacity of NEs; as an example, FEMA P[24–27] supplies fragility parameters associated with a wide range of (traditional) NEs, which were also revised/improved in recent studies.[28]

Several studies investigated the seismic response and fragility of NEs, but the literature is quite fragmented and does not provide systematic and generalizable applicable data. The amplification response of NEs in terms of accelerations, which is essential for the computation of the seismic demands on NEs, is investigated only in few cases and for very specific elements. The available fragility curves are often referred to specific NE arrangements and are not technically and scientifically correlated to the key features of NEs. Furthermore, the literature studies often assessed fragility curves only accounting for the record-to-record uncertainty, without considering other key features, such as the modeling uncertainty and the influence of the dynamic properties of NEs.

The present study provides a comprehensive assessment of the seismic response and capacity of a wide range of acceleration-sensitive NEs. The case study consists in building NEs that are fixed to the structure (e.g., floor-anchored) and that can be modeled by relatively ductile elastic-plastic single-degree-of-freedom (SDOF) systems. The assessment is based on the implementation of incremental dynamic analysis (IDA) considering advanced elastic-plastic models and building floor motions (reinforced concrete [RC] buildings). The influence of these latter on the dynamic properties of the investigated NEs, component amplification factor (CAF), and fragility curves are assessed. The methodology is robust and generalizable, and the findings can be extended to other compatible NEs, given their wide validity.

2 | CASE STUDY

The study focuses on acceleration-sensitive building elements that can be modeled by SDOF systems, which typically apply to several NEs. Overall, acceleration-sensitive elements are often implicitly or explicitly meant to be elastic SDOF systems,[29–31] and in very few cases the inelastic response is accounted for.[32] In particular, seismic verification of these elements is carried out considering elastic or inelastic spectra and formulations associated with building response (e.g., floor spectra[33,34]). Examples of regulation and code seismic demand formulations include but are not

TABLE 1 Structural details of the investigated models.

Model ID	Range [-]	f_a [Hz]	f_a [Hz]	b [mm]	t [mm]	h [m]	m [t]
M1a			1.02	70	3.0	4.50	0.10
M1b	I	~1.0	1.03	60	3.0	2.50	0.35
M1c			1.13	50	2.5	3.00	0.08
M2a			1.48	70	3.0	3.50	0.10
M2b	II	~1.5	1.52	60	3.0	2.50	0.16
M2c			1.52	60	2.5	3.00	0.08
M3a			2.97	70	3.0	2.20	0.10
M3b	III	~3.0	3.04	60	3.0	2.50	0.04
M3c			3.06	90	3.0	3.00	0.08
M4a			5.86	70	3.0	1.40	0.10
M4b	IV	> 3.0	7.34	80	4.0	1.50	0.10
M4c			9.02	70	3.0	1.05	0.10

limited to ASCE 7/22,[35] Eurocode 8,[36] Italian building code,[37] whereas several formulations were developed in literature studies.[29,30,34,38–40]

The case study models investigated in this study consist of relatively simple but representative systems, that is, cantilevers with applied mass at the free end. This simple model is widely applicable for acceleration-sensitive elements and also represents specific but common NEs, for example, antennas, suspended systems (e.g., ceilings or pipes), medical devices (e.g., operating lights), anchored elements (e.g., electric cabinets), and museum artifacts (e.g., statues).

Multiple models were considered to account for a reasonable amount of uncertainty associated with the dynamic properties and mechanical behavior of NEs. However, the NE model set cannot be considered to be exhaustive to account for various acceleration-sensitive NEs, and the related findings should be referred to the compatibility with modeled NE response and investigated case studies. In particular, all models have hollow square steel (HSS) sections, made of S275 steel, with fundamental elastic frequencies (f_a) ranging within 1–9 Hz, covering a representative range of typical NE frequencies.[35] The investigated models are described in Table 1, where b, t, h, and m are size dimension, thickness, elevation height, and applied mass, respectively. The models are organized in groups, corresponding to their f_a values; range I models have f_a approximately equal to 1 Hz, which represents a lower bound limit for NEs; range II and III models are associated with f_a equal to 1.5 and 3.0 Hz, respectively, whereas range IV models have f_a greater than 3 Hz, that is, equal to 5.9, 7.3, and 9.0 Hz.

3 | INCREMENTAL DYNAMIC ANALYSIS

3.1 | Modeling and numerical analysis

Prior to describing structural modeling and numerical analysis, it should be specified that implementing NE case studies and modeling that reflect a robust and generalizable seismic behavior tendency fosters more generalizable and extendable findings and data, possibly providing more scientific than technical/specific contributions. In this context, the case study NEs and the associated models refer to floor-anchored NEs that can be modeled as relatively ductile inelastic SDOF systems and that can be associated with structural parameters that have a clear physical meaning. The elastic-plastic modeling was implemented in OpenSees[41] through a phenomenological approach, that is, considering lumped plasticity. In particular, the SDOF systems were modeled by vertical in-series elements (Figure 1A), that is, a hysteretic zero-length moment-rotation spring was defined between a fixed node (Node 1) and an internal node (Node 2) having the same coordinates of the fixed node, and an elastic monodimensional element, defined between the abovementioned internal note (Node 2) and the free top node (Node 3); the elastic element had height equal to the SDOF height (h); the lumped mass (m) was applied at the free top node of the elastic element.

The Ibarra–Medina–Krawinkler (IMK) model[42–45] was assigned to the spring (Figure 1A-C), considering the formulation provided by Lignos and Krawinkler[46] for the determination of the backbone and hysteretic parameters associated

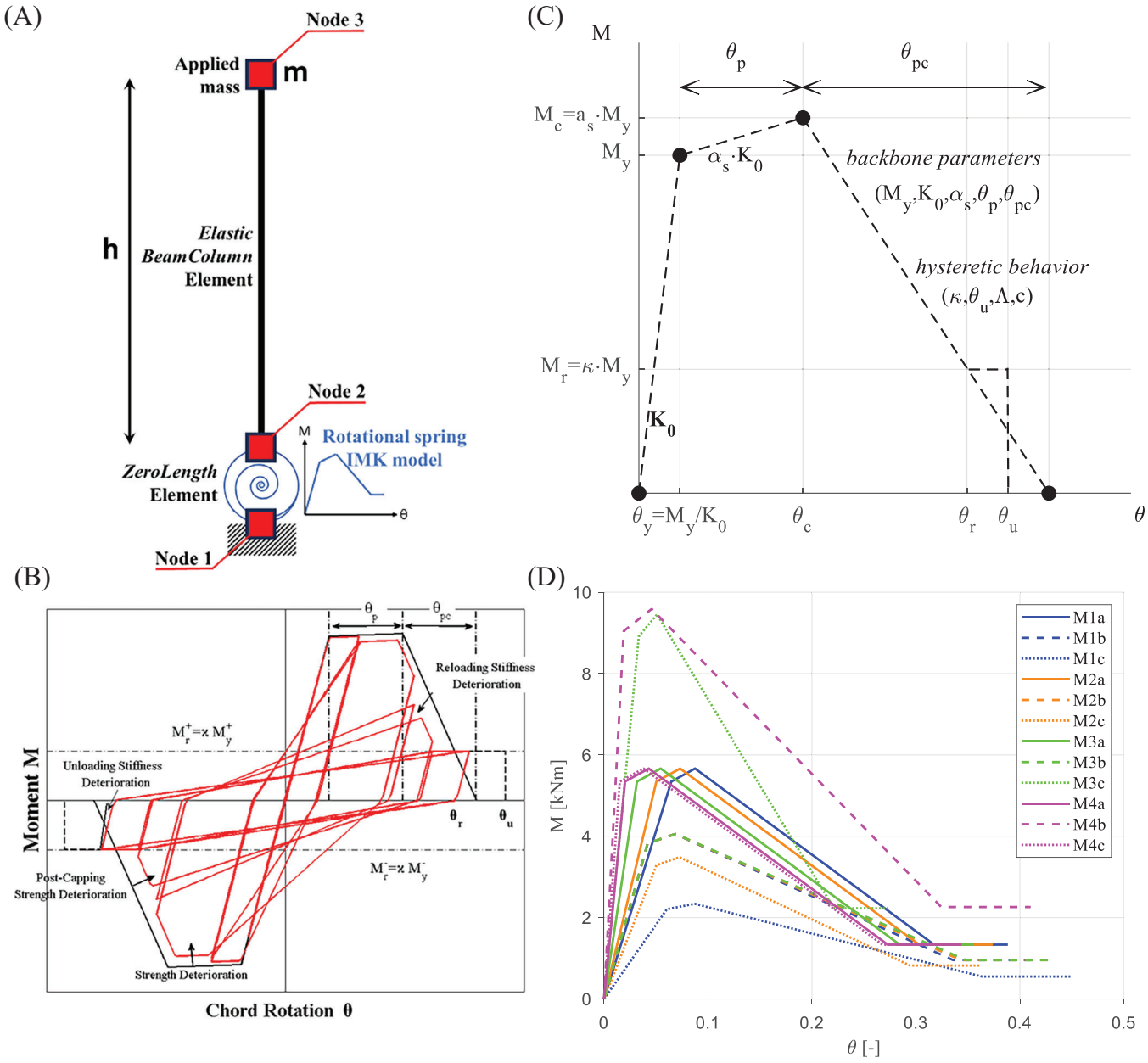

FIGURE 1 Numerical modeling: (A) structural modeling scheme (in-series element), (B) IMK model and schematic cyclic response (as provided in OpenSees),[42,44,45] (C) backbone schematic and hysteretic parameters,[47] and backbone curves of the investigated SDOF models.

with HSS columns. The elastic stiffness of both spring and elastic element was assigned so as to have a ratio of the two elements' stiffness equal to ten, resulting in a global in-series stiffness equal to the member's stiffness, according to the literature (Refs. 43, 47). *UniaxialMaterial ModIMKPeakOriented zerolength* and *ElasticBeamColumn* elements were used to model the spring and the elastic elements, respectively. The backbone behavior can be defined by yielding moment (M_y), elastic stiffness (K_0), ratio of hardening to elastic stiffness or strain hardening ratio (α_s), precapping rotation (θ_p), postcapping rotation (θ_{pc}), and by the degraded parameters, that is, ratio of residual and yielding moment (κ) and the ultimate rotation (θ_u); θ_y is the yielding rotation, M_c (θ_c) is the capping moment (rotation), a_s is the ratio of M_c and M_y, M_r (θ_r) is the residual moment (rotation). Figure 1B,C depict the backbone response. The hysteretic/degradation stiffness/strength parameters are defined by λ and c, considering four deterioration modes, that is, strength, stiffness, postcapping stiffness, and reloading stiffness ones. Finally, D defines the (a)symmetrical hysteretic behavior along the positive/negative loading directions, which can be set equal to one for symmetric response. The median values of the mechanical properties and parameters were considered, as it is typically done for advanced numerical analyses (Ref. 48). This was motivated by the

fact that the structural properties of S275 HSS elements are reasonably associated with a relatively low uncertainty due to the highly controlled industrial production processes. However, it would have been interesting also accounting for the abovementioned source of uncertainty in the analyses. Further details regarding the modeling and formulation can be found in refs. 42, 43, 46, 49.

The formulation of the rotational inelastic capacities (θ_p and θ_{pc}) and cyclic degradation parameter (Λ) was developed by Lignos and Krawinkler,[46] who performed a multivariate regression of experimental data on HSS columns; the database included more than 120 HSS columns subjected to combined axial and lateral cyclic loading. In particular, the rotational capacities were expressed as a function of identified dimensionless key parameters, that is, section parameter (b/t), applied axial force (N/N_y), and yielding strength ($C\,\sigma_y/380$). The empirical formulation associated with the calibrated response parameters X is depicted in Equation (1), and N, N_y, σ_y, and C are applied axial force, yielding axial force, yielding strength, and stress strength conversion coefficient; this latter is equal to one if σ_y is expressed in MPa; the denominator of the dimensionless yielding strength corresponds to the nominal strength of typical steel used for tubular section in Japan.

$$X = a\left(\frac{b}{t}\right)^{b}\left(1-\frac{N}{N_y}\right)^{c}\left(\frac{C\cdot\sigma_y}{380}\right)^{d} \tag{1}$$

{a,b,c,d} are equal to {0.614,−1.05,1.18,−0.11}, {13.82,−1.22,3.04,−0.15}, and {3012,2.49,3.51,−0.20} for X corresponding to θ_p, θ_{pc}, and Λ, respectively. These coefficients are applicable if (a) b/t is within 20 and 60, (b) N/N_y is within 0 and 0.5, and (c) σ_y is within 276 and 500 MPa. The yielding parameters were assessed considering the elastic properties of the models, provided by handbooks. κ was set equal to 0.25 according to Lignos and Krawinkler,[46] and this is also compliant with previous literature studies carried out by Kecman.[50] Figure 1D shows global backbone response associated with the investigated models. The geometric nonlinearities, or P-Δ effects, are implemented in the analysis. Rayleigh damping was assigned to the elastic elements, assuming a damping ratio equal to 5%.[47,51]

Incremental analyses were performed considering PFA as an IM and lateral mass displacement Δ as an EDP. The analyses were carried out from PFA equal to 0.05 g up to failure of all models, without considering structural resurrection.[52] Two types of acceleration records were selected for the numerical analyses: floor motions (FMs) and shake table protocol inputs (STPIs), which are described in the following sections.

3.2 | Floor motions (FMs)

A number of 18 FMs were selected from Center for Engineering Strong Motion Data (CESMD)[53] database and have the following characteristics: (a) PGA is greater than 0.05 g to exclude excessively mild earthquakes, (b) they were recorded in RC buildings in the US, designed/built from 1923 to 1975, (c) they correspond to the maximum amplified acceleration response over the building recording locations (almost always corresponding to roof). The entire set of FMs, namely FM set, had mean, median, standard deviation values related to PGA (PFA) equal to 0.139, 0.219, and 0.160 g (0.356, 0.465, and 0.355 g), with minimum and maximum values equal to 0.066 and 0.66 g (0.093 and 1.24 g), respectively. PFA to PGA ratio ranged from 1.156 to 4.133, with a mean, median, and standard deviation equal to 1.848, 2.179, and 0.894, respectively. The ground motions related to FM set included nine near-field and nine far-field records, where 15 km was considered as a threshold distance to the epicenter (Ref. 54). Near- and far-field FM records define NFFM and FFFM sets. FM set includes seven records having PGA greater than 0.20 g (e.g., strong records), corresponding to strong floor motion (SFM) set. Low-, medium-, and high-rise buildings were equally considered within FM set (i.e., six records each), and the related records define LRFM, MRFM, and HRFM sets, respectively. FM set corresponds to FM #1, #2, #3, #5, #6, #7, #9, #10, #12, #13, #14, #15, #17, #18, #19, #21, #22, #23 records considered in ref. 21 (FM #4, #8, #11, #16, #20, and #24 were not considered in this study since they were preliminary found to be excessively mild with regard to case study models). The i^{th} and statistical spectral responses of the defined FM sets are depicted in Figure 2A, considering PFA equal to 1.0 g. It should be specified that the number of considered records, although compatible with record suite sizes used in past studies,[21,55,56] cannot be considered to be exhaustive and comprehensive for fully accounting for both hazard and building seismic uncertainties. Therefore, the associated findings have to be interpreted and implemented in compliance with the relatively limited number of records, and they could be extended to other case studies with due consideration.

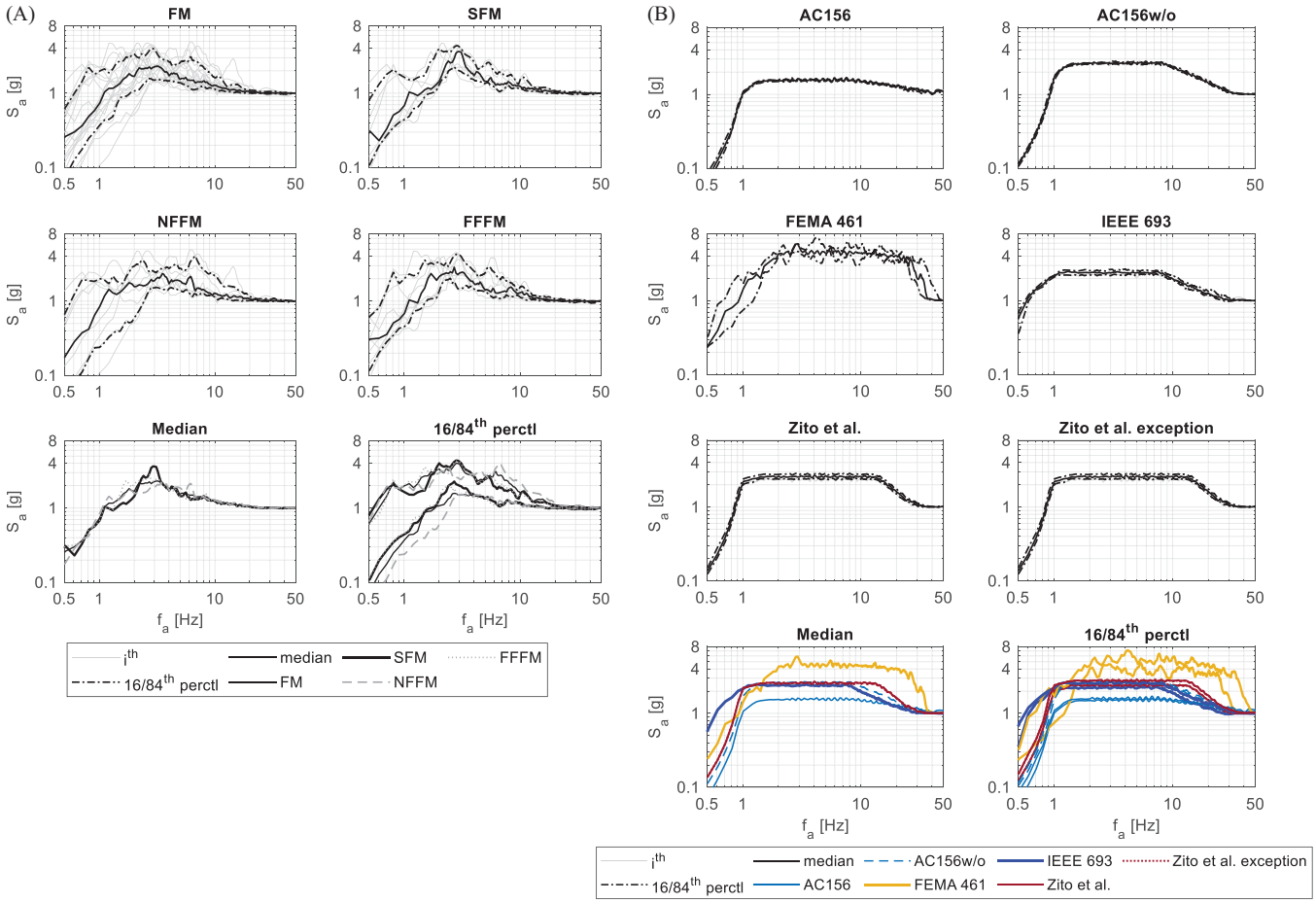

FIGURE 2 Spectral pseudoacceleration response (S_a) over frequency associated with (A) floor motion (FM) sets and (B) shake table protocol input (STPI) sets, considering peak floor acceleration (PFA) equal to 1.0 g; both S_a and f_a are plotted considering logarithmic scale.

3.3 | Shake table protocol inputs (STPIs)

STPIs are defined as artificial inputs compliant with the most authoritative shake table protocols (STPs) for seismic assessment and qualification/certification of acceleration-sensitive elements.[9] AC156,[57] FEMA 461,[58] IEEE 693,[59] and Zito et al.[60] STPs were considered. An enhanced version of AC156,[57] namely AC156w/o, and a peculiar application of Zito et al.,[60] namely Zito et al. (1 Hz) exception, were also investigated. Further details regarding the existing protocols are omitted for the sake of brevity. AC156w/o protocol consist in AC156 without assuming the upper bound limit for $A_{FLX\text{-}H}$, equal to 1.6 S_{DS}. As a matter of fact, few recent studies[21,61,62] suggested that such a limitation might represent a detrimental measure in terms of representativity of the seismic demands associated with AC156 protocol. Zito et al. exception protocol consists in applying exceptions in developing Zito et al. protocol input, as it is defined in[9]; in particular, the signal was defined by removing the baseline waveform frequency corresponding to 1 Hz but enforcing the spectrum-compatibility over the whole protocol range of frequencies (i.e., including 1 Hz). This assumption follows the hypothesis that the removed frequencies (in the vicinity of 1 Hz) are particularly critical in terms of signal reproducibility and resonance phenomena. This hypothesis might often be applicable in real cases due to shake table displacement limitations and potential resonance phenomena.[10,60,63]

A set of accelerograms was generated or selected for each investigated protocol: three records for FEMA 461, seven records for AC156, AC156w/o, Zito et al., and Zito et al. exception, and ten records for IEEE 693. Two FEMA 461 records were directly provided by the protocol, whereas a record was generated in D'Angela et al.,[61] according to Wilcoski et al.[64] AC156 and AC156w/o records were generated according to,[10] considering z/h equal to one, where this latter parameter describes the ratio of the elevation eight of NE and the building elevation height. Seven records were developed considering Zito et al. and Zito et al. exception, by implementing the procedure provided in ref. 60 (z/h equal to one).

Finally, both empirical- and artificial-based signals were selected according to IEEE 693 protocol, considering peak displacements limitations of 200 mm.[63] The shake tables of the University of Naples Federico II (Ref. 65) were considered as a reference to check or enforce the compatibility and the reproducibility of the signals. Figure 2B shows the spectral pseudoacceleration response (S_a) as a function of frequency (f_a) associated with STPI sets, assuming PFA equal to 1.0 g.

3.4 | Fragility analysis

The fragility curves associated with the response of the reference models are assessed according to,[7,66] that is, using an IM-based lognormal model (Porter *method A*). The fragility median value and logarithmic standard deviation are defined x_m and σ, respectively. The only record-to-record (RTR) uncertainty was considered. x_m and σ were estimated according to (2) and (3), respectively. In particular, N represents the number of records and r_i is the IM capacity value corresponding to the i^{th} record, related to the achievement of a specific DS.

$$x_M = \exp\left(\frac{1}{N}\sum_{i=1}^{N}\log(r_i)\right) \tag{2}$$

$$\sigma = \sqrt{\frac{1}{N-1}\sum_{i=1}^{N}\left[\log\left(\frac{r_i}{x_M}\right)\right]^2} \tag{3}$$

The quality of fitting was assessed according to Porter et al.[7,66,67] Considering Porter *method A*, a high fragility function quality level is related to the case in which all following conditions are verified: (H1) peer-reviewed publication of the data, (H2) number of specimens, or equivalently, records, is greater than or equal to five, and (H3) Lilliefors test[68] pass at 5% significance level; it is specified that it should be examined and justified (H4) differences of greater than 20% in x_M or σ, compared with past estimates and (H5) any case of $\sigma < 0.2$ or $\sigma > 0.6$. The quality of fitting is considered to be moderate if (M1) the number of specimens, or records, is greater than or equal to three; furthermore, (M2) case with $\sigma < 0.2$ or $\sigma > 0.6$ should be examined and justified.

PFA was considered as an IM, and the horizontal displacement of the concentrated mass Δ was assumed as an engineering demand parameter (EDP). The fragility was estimated considering multiple DSs, identified by the exceedance of thresholds of Δ correlated with relevant DSs, referring to the backbone response including P-Δ effects (Figure 1B). The investigated DSs are: DS1, that is, halved yielding displacement/strength; DS2, that is, yielding displacement/strength; DS3, that is, displacement associated with capping strength; DS4, that is, displacement associated with a strength drop of 20% from the capping condition; DS5, that is, displacement associated with the achievement of the residual strength or onset of perfectly plastic residual response. The displacement capacity thresholds (Δ_{DS}) and the ratios between them and the DS5 capacity (Δ_{DS}) are plotted in Figure 3. DS1 is associated with functioning of NEs, DS2 is representative of damage limitation, DS3 is associated with life safety conditions, and DS4/DS5 are compatible with near collapse condition.

4 | RESULTS AND DISCUSSION

4.1 | IDA curves

Figures 4 and 5 show median and 84^{th} percentile IDA curves, respectively, using PFA as an IM and dimensionless displacement (Δ/Δ_{DS5}) as an EDP, corresponding to single models and grouped range models. The statistical curves were obtained by fixing PFA values and estimating the statistical Δ/Δ_{DS5} values over the set of IDA curves. The 84^{th} percentile curves are meant as Δ/Δ_{DS5} values, for given PFA, below which 84^{th} of score falls; this represents a more conservative reference, that is, considering a higher input severity. The comparison between the median and 84^{th} percentile response allows identifying the dispersion of the single input IDAs within the different loading history sets, even though in a qualitative manner. However, the data dispersion associated with the seismic response of the investigated models is addressed in a more quantitative and explicit manner in the framework of the fragility assessment. Therefore, in this section, no explicit comments are reported regarding the data dispersion for the sake of redundancy.

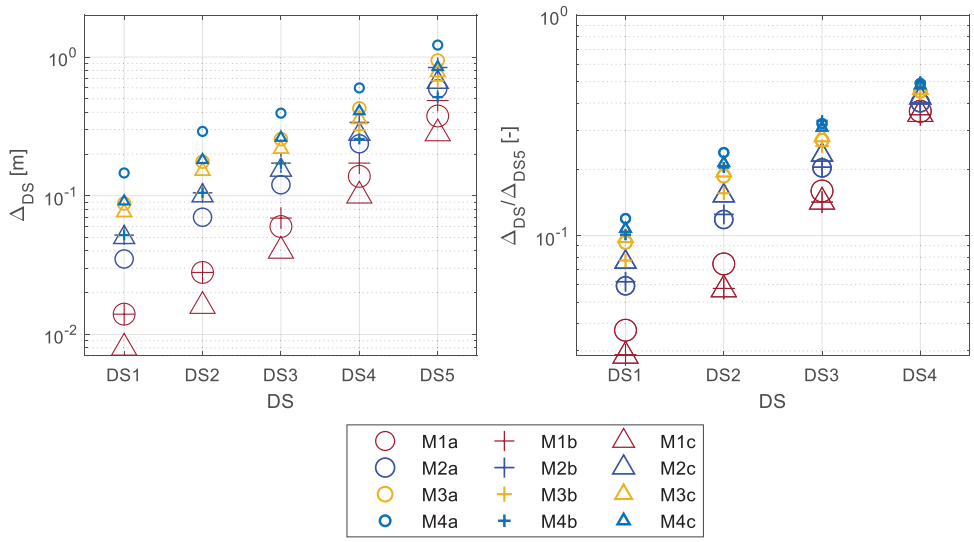

FIGURE 3 Displacement capacities (Δ_{DS}) and displacement capacities divided by DS5 capacity (Δ_{DS}/Δ_{DS5}) for all models.

The results are discussed in terms of the influence of loading history set and model features on the seismic response, also expressed as input/response IDAs severity, where higher severity is associated with larger EDP for given PFA or, equivalently, lower PFA for given EDP.[69] In particular, protocol input IDA responses are discussed considering FM ones as a reference, explicitly referring to the investigated model features (especially frequency ranges).

Severity patterns associated with the different loading histories can be observed. IEEE 693 (FEMA 461) inputs are the most severe for ranges 1 and 2 (3 and 4) models considering both median and 84th percentile response, even though, in this latter case, IEEE 693 responses are quite similar to FEMA 461 for some models (e.g., M1c and range 3 models). Considering median responses, IEEE 693 is overall significantly more severe than FM results, especially for ranges 1 and 2, where PFA values associated with unitary Δ/Δ_{DS5} is even lower than half FM ones. While FEMA 461 fits quite well with range 1 FM curves, the protocol also provides significantly more severe curves, if compared to FM, which are even more severe than IEEE 693 for ranges 3 and 4. A different trend is exhibited for both IEEE 693 and FEMA 461 protocols if 84th percentile curves are considered. As a matter of fact, both protocols fit quite well, erring on the side of caution, FM curves for ranges 1–3, whereas the response is still extremely conservative for range 4 models. AC156 is overall the least severe protocol over the investigated protocols, as it was also found with regard to rigid block dynamics[21,69] and was discussed in previous studies.[30,34,62,70] Considering median (84th percentile) curves, AC156 is often (always) less severe than FM and other protocol responses. In particular, median AC156 curves are less severe than FM ones for ranges 1 and 2, over relatively large Δ/Δ_{DS5} values (e.g., $\Delta/\Delta_{DS5} > \sim 0.4$–$0.5$), and for ranges 3 and 4, overall and especially in the postyielding response. In some cases, 84th percentile PFA values associated with unitary Δ/Δ_{DS5} are even greater than twice the FM ones, for example, ranges 1 and 2.

For ranges 1 and 2, median curves related to Zito et al. inputs are quite similar to FEMA 461 curves and quite similar to IEEE 693 ones over $\Delta/\Delta_{DS5} < \sim \Delta_{DS3}/\Delta_{DS5}$ curves, whereas, for Δ/Δ_{DS5} larger values, they are less severe than IEEE 693; but, overall, they are more similar to or more severe than FM ones. Zito et al. 84th percentile curves related to ranges 1 and 2 are similar to FEMA 461 and IEEE 693 and FM curves over relatively smaller Δ/Δ_{DS5} values, for example, $\Delta/\Delta_{DS5} < \sim 0.2$–$0.4$, whereas they are less severe for larger values. Considering single range 3 models, Zito et al. curves are close to FM ones. Similarly, Zito et al. curves are significantly more compatible with FM ones than IEEE 693 and FEMA 461 considering range 4 models. In particular, Zito et al. protocol curves err on the side of caution up to $\Delta_{DS3}/\Delta_{DS5}$, whereas they slightly overestimate PFA values for larger values, still enveloping quite well FM curves. Considering 84th percentiles, Zito et al. protocol is significantly less severe than FM curves for range 1 models and $\Delta/\Delta_{DS5} > 0.5$, whereas it envelops much better FM results for all other ranges, especially up to $\Delta_{DS3}/\Delta_{DS5}$ response. Zito et al. exception curves are quite similar to Zito et al. ones, proving that the frequency content adjustment does not affect the severity of the protocol, even in the case of range models which have an elastic frequency that is approximately equal to the adjusted frequency value (i.e., 1 Hz). Both median and 84th percentile IDAs related to AC156w/o are overall quite similar to Zito et al., oscillating around the latter protocol.

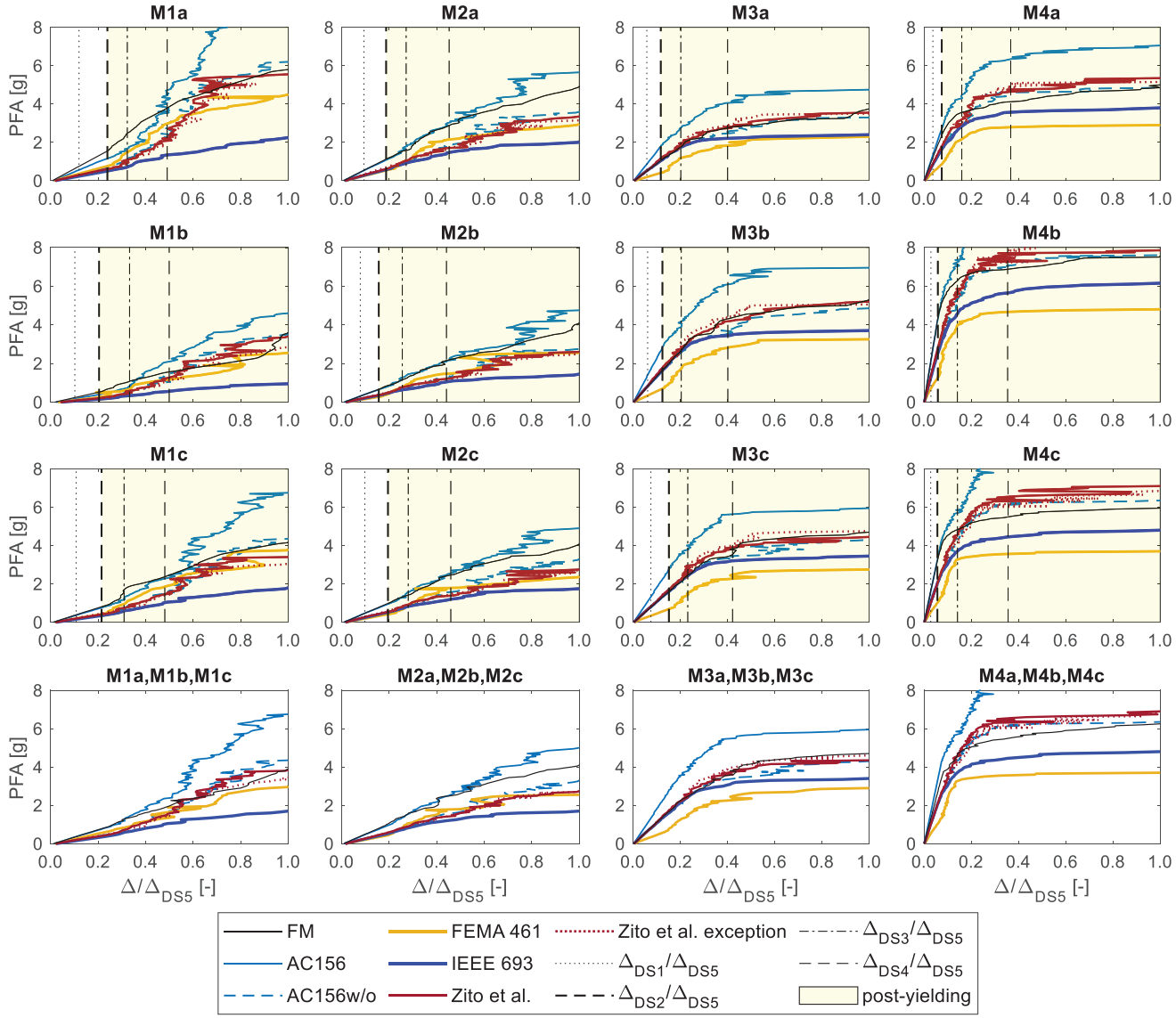

FIGURE 4 Median IDA curves (peak floor acceleration (PFA) as a function of dimensionless displacement (Δ/Δ_{DS5})) associated with all loading history sets, corresponding to single models and grouped range models.

4.2 | Component amplification factor (CAF)

Component amplification factor (CAF) is defined as the absolute ratio between the peak component acceleration (PCA), registered on the component mass, and PFA. The significance of CAF is more traditionally associated with the elastic response rather than with the inelastic one. However, recent codes[35,37] and literature studies[71,72] account for the influence of the inelastic incursion, or equivalently, of the NE ductility capacity, on acceleration amplification or seismic NE response in general (e.g., through concept of behavior factor). In particular, it should be noted that the significance of CAF in terms of elastic or inelastic response is strongly associated with the component and performance level of interest. If the interest of the seismic safety assessment of the case NE is focused on operational/functional performance conditions, CAF can be referred to the elastic response and the assessment verification can be based on acceleration/force measures. Conversely, if the interest is on damage limitation or severe damage conditions and NE retains ductility capacities, CAF of interest can be associated with inelastic (or, more generally, nonlinear) response. However, assessment of inelastic response is typically carried out considering deformation- or ductility-based measures/approaches instead of acceleration/force ones[72,73] Accordingly, the meaning of CAF is generally less significant over these latter performance levels and NE responses, even though these aspects are scientifically relevant.

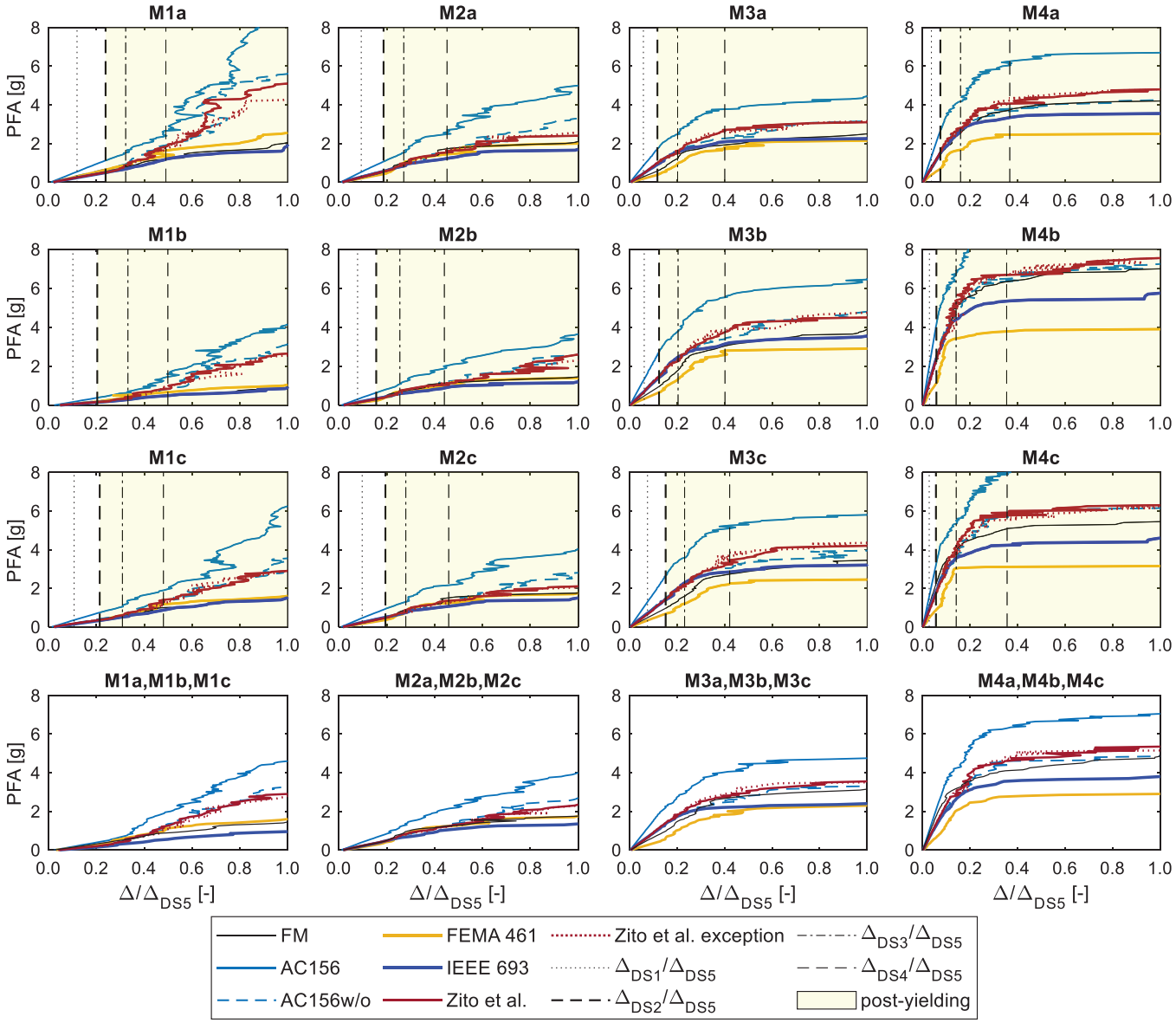

FIGURE 5 84th percentile IDA curves (peak floor acceleration (PFA) as a function of dimensionless displacement (Δ/Δ_{DS5})) associated with all loading history sets, corresponding to single models and grouped range models.

Figure 6 shows the median component amplification factor (CAF) as a function of PFA The 84th percentile CAF is depicted in Figure 7 for the sake of completeness; the results are depicted up to PFA equal to 5 g. In many cases, CAF has a relatively regular trend: (a) first plateau branch up to PFA values that increase as the model frequency increases due to the increasing yielding PFA capacity, (b) relatively regular decreasing branch up to PFA values that increase as the model frequency increases due to the increasing of the inelastic PFA capacity, and (c) sudden drop to a null value is associated with the achievement of failure or instability (for median (84th percentile) curve, the drop is associated with a 50% (84th) failure/instability occurrences).

The maximum CAF and its trend are strongly conditioned by the considered input sets, combined with the frequency of the model. All input sets but FEMA 461 and FM show a trend that does not significantly depend on the models. In particular, CAF values defining the above mentioned branches do not vary as the model changes but the corresponding PFA tends to increase as the frequency increases. This is due to the fact that PFA capacities related to the key response states (elastic limit, capping capacity, and residual capacity) increase as the frequency of the model grows (e.g., see IDA curves in Section 4.1). In other words, the CAF vs. PFA response related to these protocols tends to elongate, in terms of PFA, as the frequency of the models increases, approximately keeping the same ordinate values.

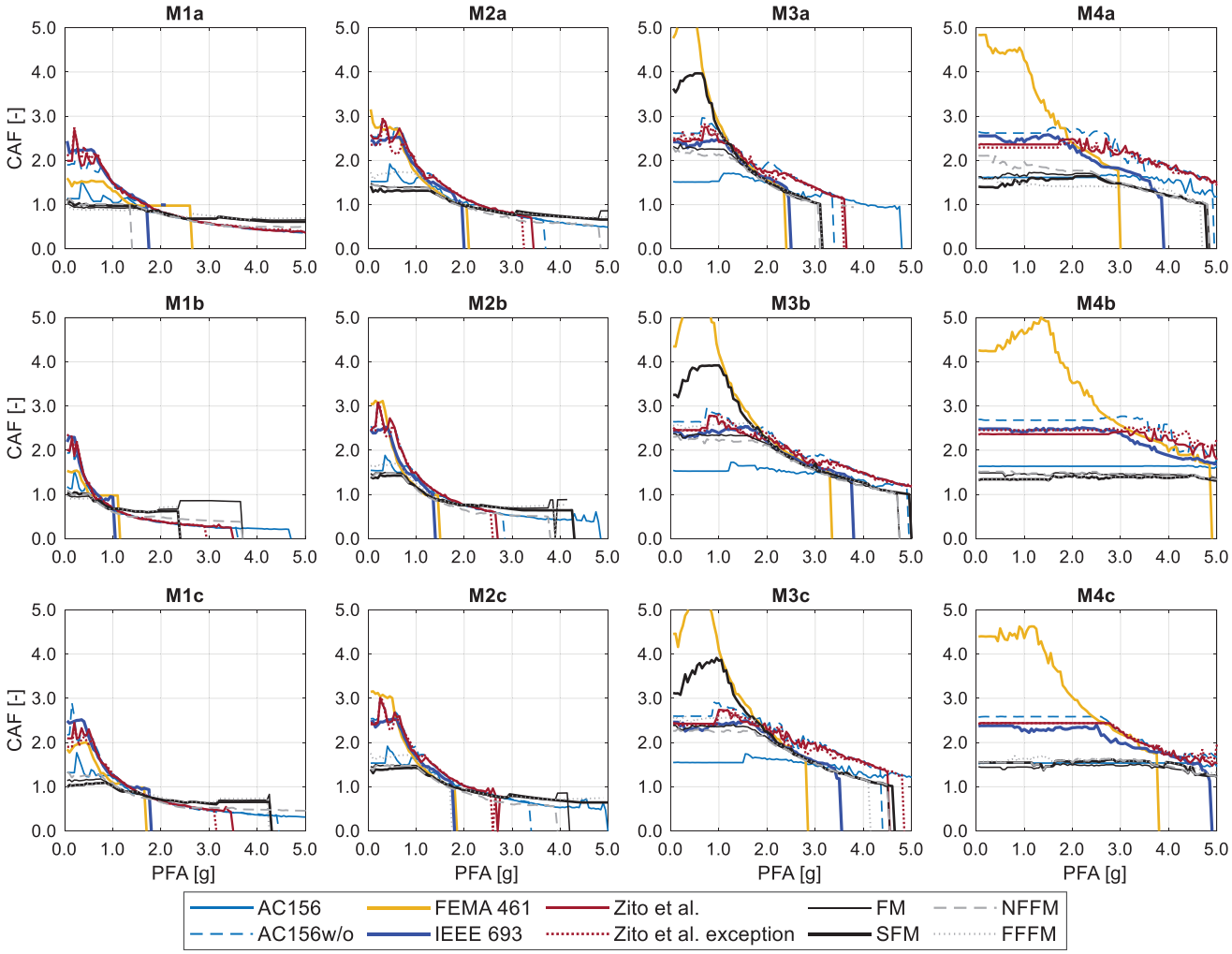

FIGURE 6 Median component amplification factor (CAF) as a function of peak floor acceleration (PFA) associated with all loading history sets and models.

For the other input sets, that is, FM and FEMA 461, the elongation is observed but there is a variation in the CAF values, and the variation depends on the input sets. FM CAF values tend to increase passing from models M1 to M2 and from M2 to M3, especially over the elastic response, whereas models M4 values are more comparable with models M2 (i.e., CAF decreases from M3 to M4). FEMA 461 shows a trend similar to FM: CAF tends to increase as frequency increases from models M1 to M3, and a minor decrease is found passing from M3 to M4. M4 CAF is more similar to M3 ones rather than to M2. This means that the acceleration amplification due to all protocols but FEMA 461 does not significantly depend on the frequency of the model, whereas FEMA 461 protocol and FM inputs are associated with (a) an increasing acceleration amplification as the frequency increases over 1–3 Hz and (b) a decreasing amplification within 3–9 Hz.

Zito et al., Zito et al. exception, AC156w/o, and IEEE 693 show a very similar response among them, especially considering the maximum CAF values and over the decreasing branch. AC156 protocol provides maximum CAF values that are significantly lower than the other protocols, and, in many cases, especially over models M1 and M2, AC156 decreasing branch tends to match the other protocols. FM inputs are associated with maximum CAF values that are matched quite well by AC156 over M1 and M2 models, being significantly lower than all other protocols. For models M3, FM is enveloped very well by Zito et al., Zito et al. exception, AC156w/o, and IEEE 693, whereas AC156 protocol (FEMA 461) is associated with significantly lower (higher) CAF values. For models M4, AC156 again matches relatively well FM inputs, being significantly lower than all other protocols.

A more operative elaboration of the CAF results is provided in Figure 8, which reports both (a) median and (b) 84th percentile CAF associated with DS1 (i.e., CAF_{DS1}), as a function of f_a, for all FM sets. The response associated with all

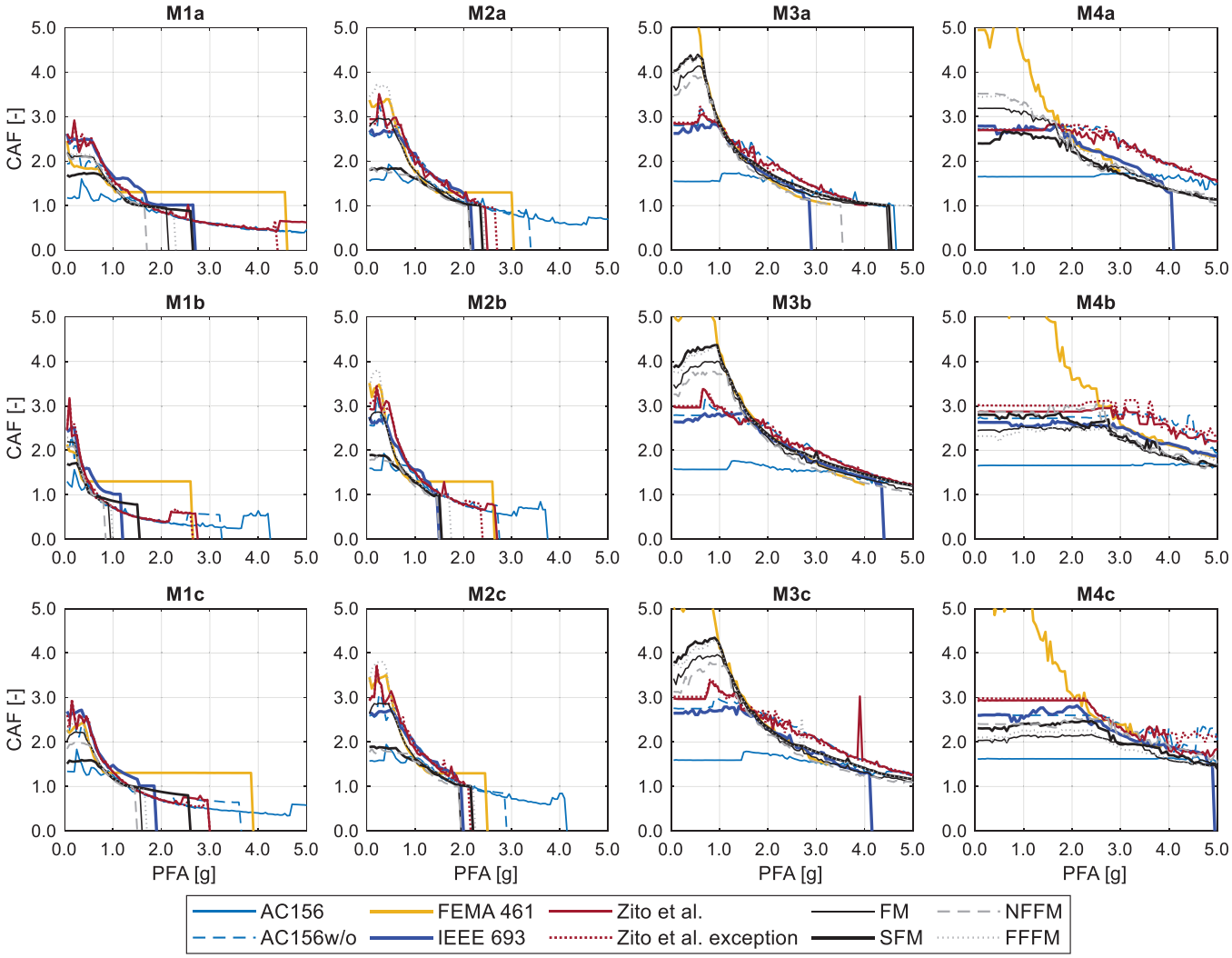

FIGURE 7 84th percentile component amplification factor (CAF) as a function of peak floor acceleration (PFA) associated with all loading history sets and models.

FM subsets are reported: (all) FM, SFM, NFFM, FFFM, LRFM, MRFM, and HRFM. Figure 8 supplies robust estimations for CAF to be used to quantify (elastic) seismic demand on a wide range of NE frequencies, specifically aimed at seismic verification of operational/functional performance levels. The results associated with DS2 condition were approximately identical to the DS1 ones, and they are not reported in the paper. Similar graphs referred to the inelastic CAF thresholds could be derived from the provided figures (e.g., Figure 6 for medians). As it was qualitatively highlighted in Figure 6, maximum CAF, which are associated with the elastic response, associated with FM sets depends on the frequency of the model.

A general trend can be identified over all FM sets: CAF increases as f_a grows within 1–3 Hz and it tends to decrease for larger values, even though there are exceptions. In particular, the decreasing trend is more evident considering the 84th percentiles responses, and for the medians CAF response within 6–9 Hz is less conditioned by f_a. Considering the median response, the only difference found between FM and SFM response is related to CAF value associated with 3 Hz frequencies, that is, the most amplified acceleration response; in particular SFM CAF is significantly greater than FM CAF. This does not occur considering the 84th percentiles since SFM CAF is just greater than FM one and FM CAF associated with frequencies lower than 3 Hz is larger or significantly greater than SFM one. These results can be motivated by looking at the comparisons among the spectral responses, depicted in Figure 2A: median SFM ordinates corresponding to 3 Hz is greater than FM one, whereas 84th percentile curves associated with FM are greater than SFM ones within 1–1.5 Hz. This implies that, on average, SFM are more severe than FM, in terms of elastic acceleration amplification, only for 3 Hz models, whereas, considering more conservative estimates, that is, 84th percentile response, FM are more severe than SFM

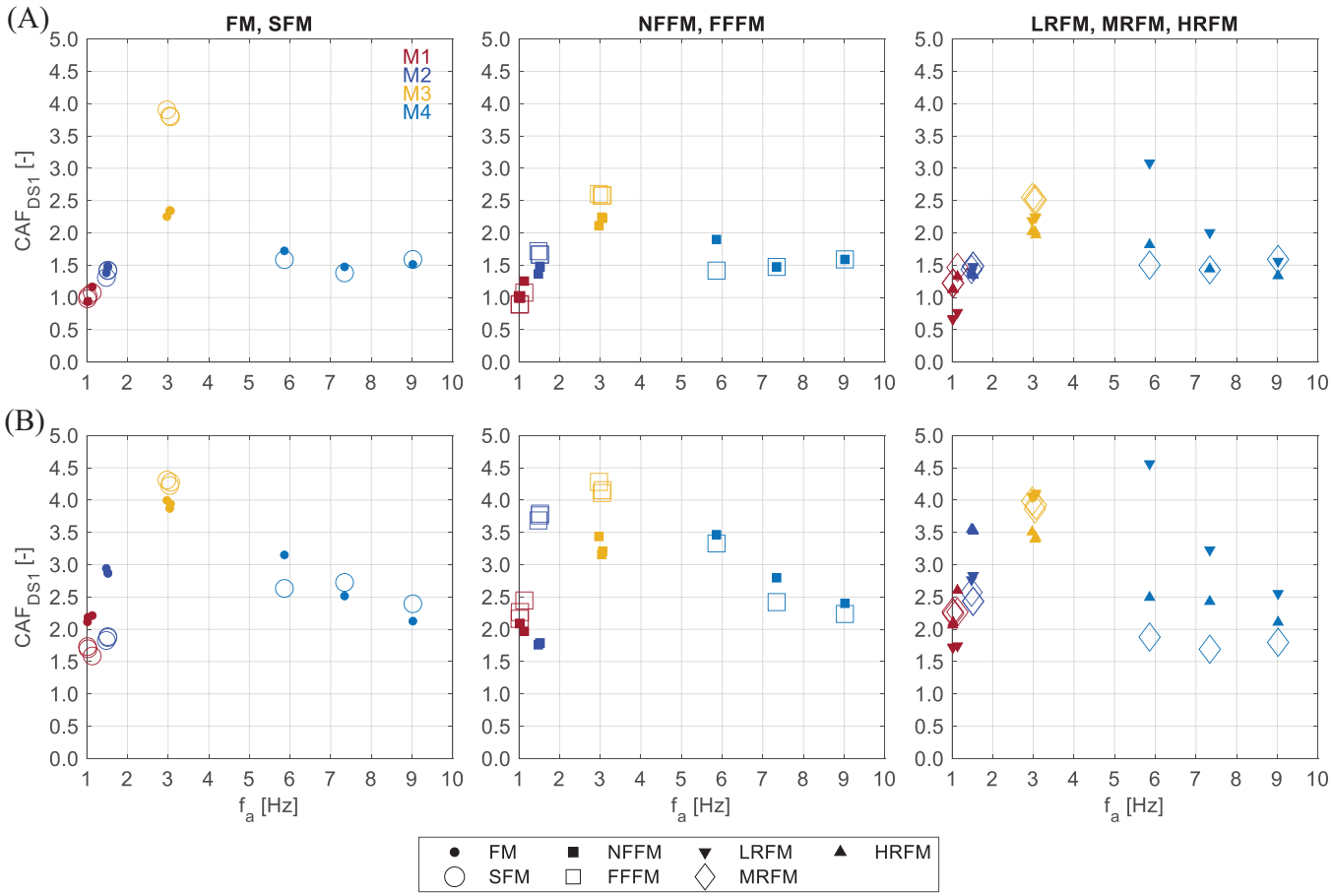

FIGURE 8 (A) Median and (B) 84th percentile component amplification factor (CAF) related to DS1 conditions (CAF_{DS1}) as a function of elastic frequency (f_a), associated with floor motion (FM) sets (FM, SFM, NFFM, FFFM, LRFM, MRFM, and HRFM sets).

for models having fundamental frequencies lower than 3 Hz. FFFM are found to be more severe than NFFM, especially within 1.5–3 Hz and for 84th percentile responses. Looking at Figure 2A, it can be seen that 84th spectral ordinate associated with FFFM is greater than NFFM ones within 1–2 Hz and at about 3 Hz. The amplification response associated with the height of the building depends on the specific frequency of interest of the model. In particular, it can be noted that LRFM sets are more severe, in terms of CAF, within 6–9 Hz, especially for 6 Hz models, and this is compatible with the fact that these signals are meant to represent buildings that are relatively rigid in terms of fundamental frequencies. For lower frequencies, it is not easy to identify clear trends, even though it is evident that median and 84th percentile MRFM and HRFM CAFs tend to overpass LRFM CAFs as expected. The response highlighted in Figure 8, especially regarding the subsets associated with the building height, might depend on the specific signals that were selected, and it might not be simply generalized or extrapolated. It is worth noting that the median CAF associated with LRFM sets is lower than one corresponding to 1 Hz models, and this is compatible with the fact that the filtering action of relatively rigid buildings might be less severe on flexible components that the one associated with less rigid buildings and/or less flexible components. Considering the median (84th percentile) response associated with FM set, the maximum CAF values, corresponding to 3 Hz, are overall just below 2.5 (4.0), whereas an upper bound limit for other frequencies could be set equal to 1.5–2.0 (2.5–3.0). However, Figure 8 could be referred to for more accurate and less conservative estimates as a function of the relevant frequencies.

It is interesting to compare the estimated CAF values and the provisions of current building codes. According to ASCE 7–16[74] and AC156 protocol,[57] CAF varies from 1.0 (rigid components, for example, f_a greater than 8.3 Hz) to 2.5 (flexible component, for example, f_a less than 8.3 Hz). Eurocode 8[36] implicitly provides CAF as a linear function of z/h, varying from 2.2, at z/h equal to zero, to 2.5, at z/h equal to one. The New Zealand document "The Seismic Assessment of Existing Buildings: Technical Guidelines for Engineering Assessments (the Guidelines) [75]" refers to the current New Zealand code NZS 1170.5:2004,[76] which expresses CAF as a linear function of the NE fundamental period, and it varies from 0.5, for f_a

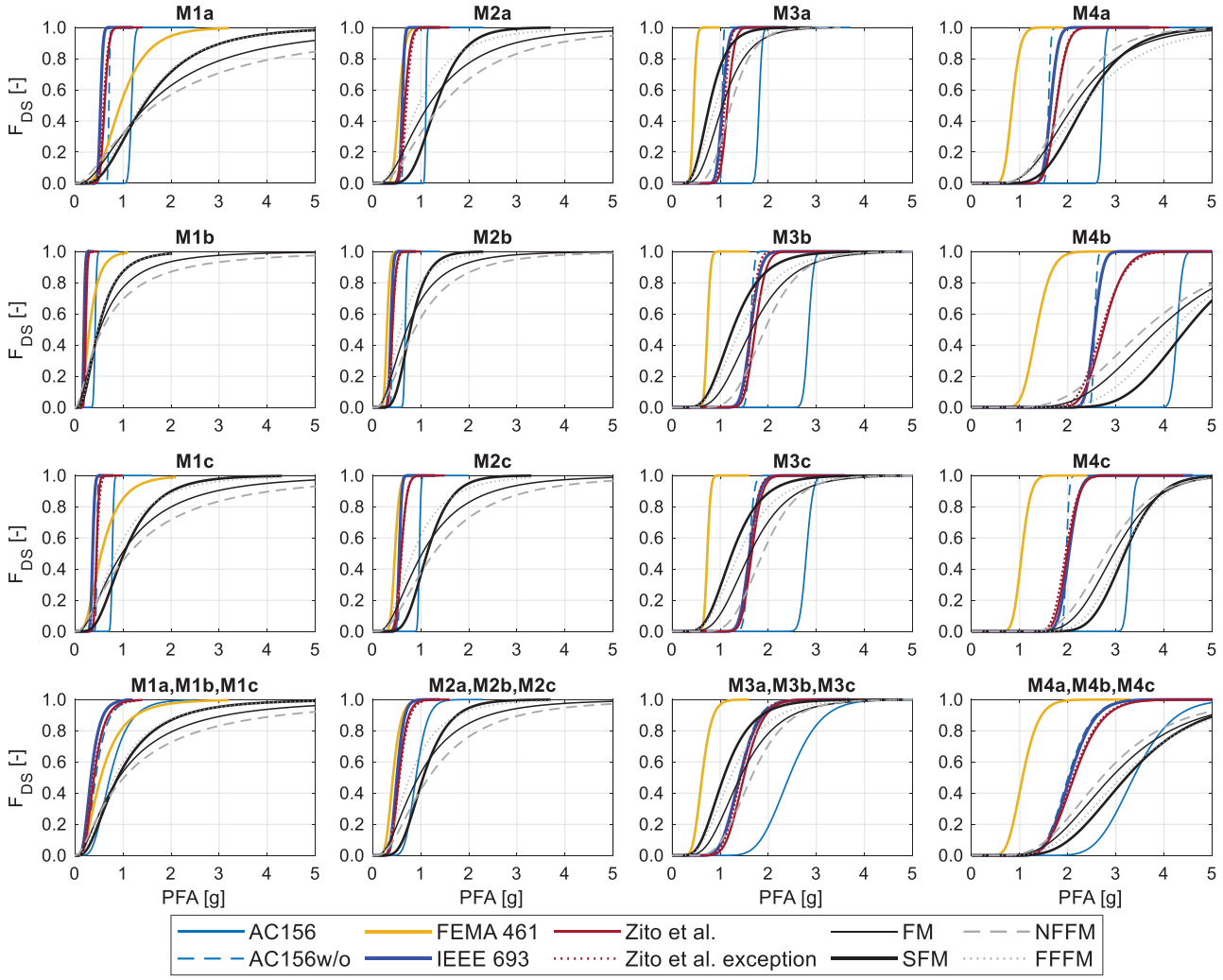

FIGURE 9 Fragility (F_{DS}) as a function of peak floor acceleration (PFA) evaluated considering DS2, associated with all loading history sets, corresponding to single models and grouped range models.

less than or equal to 0.67 Hz, and 2.0, for f_a greater than or equal to 1.33 Hz. The Italian building code,[37] with regard to the simplified formulation applicable for frame structures,[30,37,77] provides CAF as a tabular function of the fundamental building period (T_1), equal to 5.0, 4.0, and 2.5 corresponding to T_1 less than 0.5 s, within 0.5 and 1.0 s, and greater than 1.0 s, respectively. Considering median response (Figure 8A), if FM set is considered (i.e., a wide range or low to high-intensity earthquake scenarios), the abovementioned codes provide relatively safe CAF values since the maximum CAF_{DS1} value is between 2 and 2.5 (corresponding to M3 models, i.e., f_a equal to about 3 Hz). Conversely, if higher percentile measures are considered (e.g., 84th percentile response in Figure 8A) or in the case of SFM set (associated with high-intensity earthquake scenarios), CAF_{DS1} significantly grows up to values in the order to 4–5, and only NTC 2018 formulation, among the ones investigated above, provides relatively safe estimations considering T_1 lower than 1.0 s (e.g., low- and medium-rise buildings).

4.3 | Fragility curves

Figures 9, 10, 11 show the fragility curves corresponding to DS2, DS3, and DS4, respectively. IEEE 693, Zito et al., and AC156w/o, fragility curves are quite similar among them for all models, except for models M4, where IEEE 693 and AC156w/o fragilities are higher than Zito et al. In particular, IEEE 693, Zito et al., and AC156w/o fragilities are significantly higher than FM set ones, except for M3 models, where SFM fragilities are higher than the former fragilities, and for M4 models DS4, where Zito et al. fragilities are lower than FM sets ones. FEMA 461 fragilities are lower than IEEE 693,

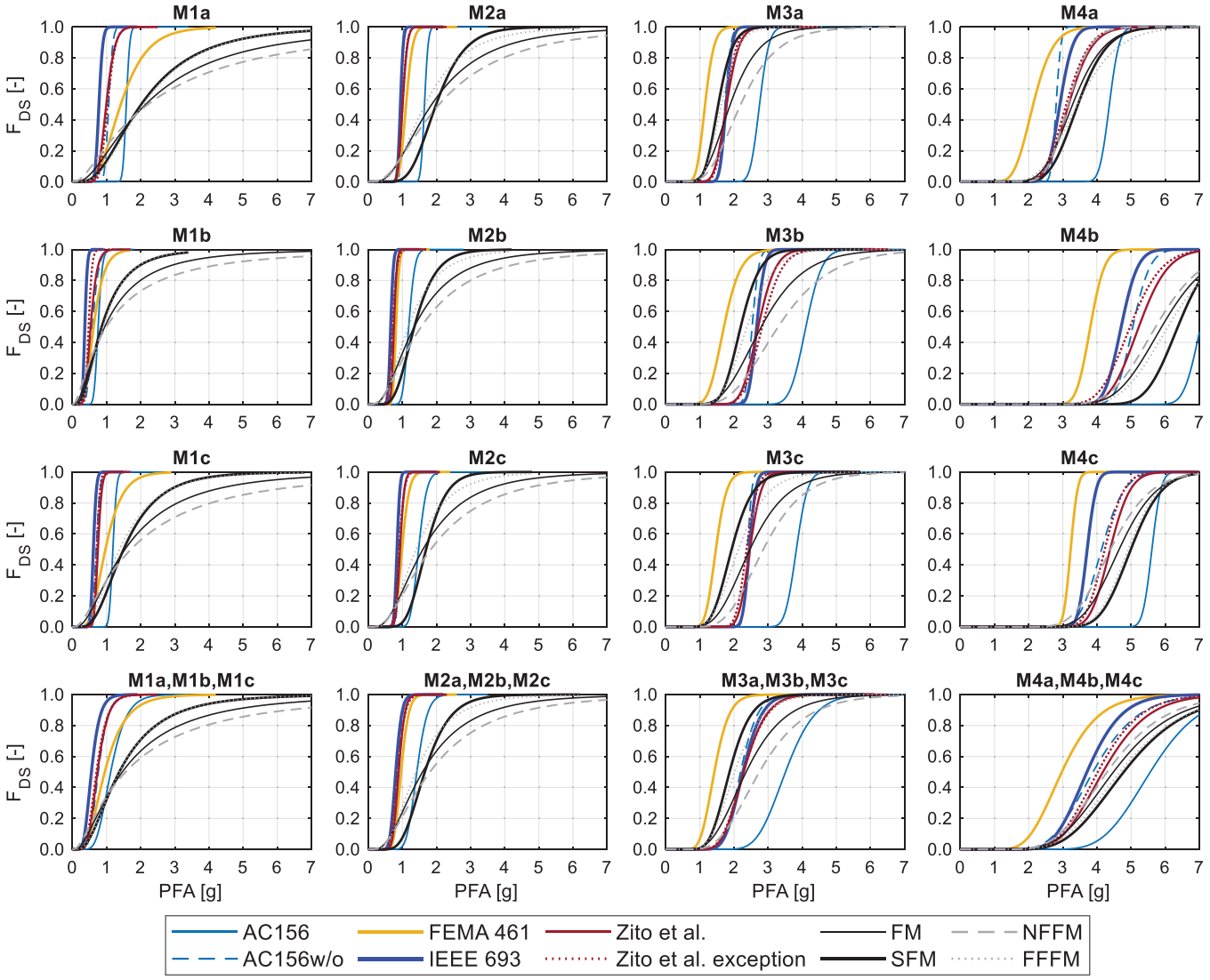

FIGURE 10 Fragility (F_{DS}) as a function of peak floor acceleration (PFA) evaluated considering DS3, associated with all loading history sets, corresponding to single models and grouped range models.

Zito et al., and AC156w/o for models M1 and M2 DS4, similar for models M2, and higher for models M3 and M4, and they are always higher than FM ones. AC156 fragilities are always lower than the other protocol fragilities, even lower than FM fragilities for models M3 and M4. Further comments regarding the evolution of the fragility parameters over the model frequencies are reported in the following.

The quality of fitting was assessed as described in Section 3.4. Regarding high-quality criteria, conditions (H1) and (H2) are verified in all cases. Regarding condition (H3), Lilliefors test is passed in about 37% and 97% cases considering FM and SFM set results, respectively; condition (H4) is not applicable (the data cannot be compared with past data) and condition (H5) should be referred to the reliability and robustness of methodology and data, assessing and evaluating the cases associated with $\sigma < 0.2$ or $\sigma > 0.6$, as discussed below. Considering FM and SFM sets, σ is within 0.2–0.6 in about 37% and 60% cases, respectively; in these cases, if Lilliefors test is passed, the quality of fitting is high (HQ); this occurs in about 28% and 57% cases for FM and SFM sets, respectively. Given the advanced numerical model and analysis and the robustness of the implemented methodology, condition (H5) is reasonably considered to be applicable to all cases but, for the sake of robustness, Lilliefors pass cases in which σ is not within 0.2–0.6 are classified as high quality but subject to checks (HQ*); this occurs in about 8% and 40% cases for FM and SFM sets, respectively. Regarding the moderate quality of fitting, condition (M1) is valid for all cases; condition (M2) corresponds to condition (H5). Lilliefors fail cases in which σ is within 0.2–0.6 are classified as moderate quality of fitting (MQ); these cases correspond to 8% and 3% for FM and SFM sets, respectively. Lilliefors fail cases with σ not within 0.2–0.6 are associated with moderate quality but subject to checks

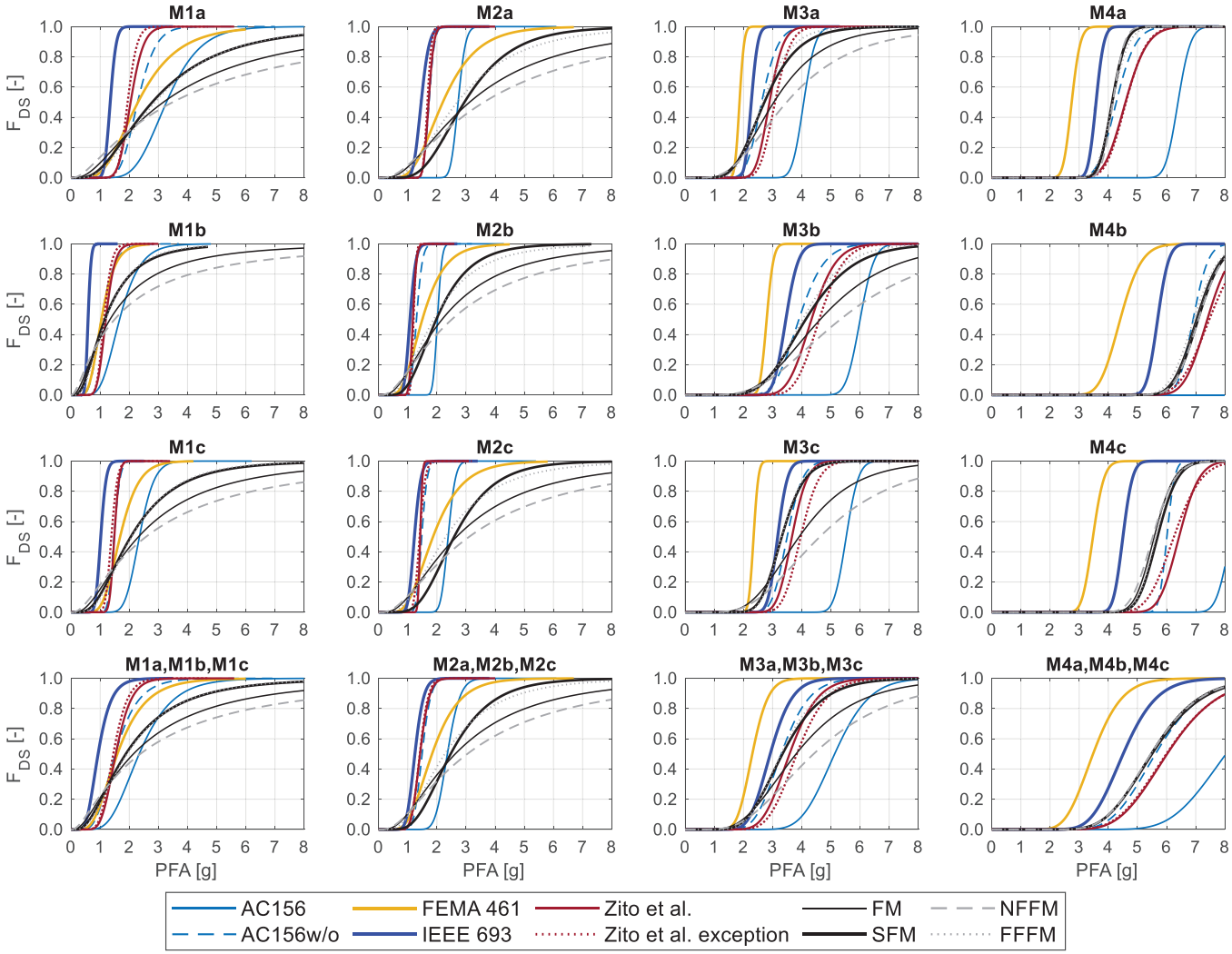

FIGURE 11 Fragility (F_{DS}) as a function of peak floor acceleration (PFA) evaluated considering DS4, associated with all loading history sets, corresponding to single models and grouped range models.

TABLE 2 Quality of fitting associated with all floor motion (FM) and strong floor motion (SFM) sets, according to Porter et al.[7,67]; HQ, HQ*, MQ, and MQ* correspond to high quality fitting, high quality fitting subject to checks, moderate quality of fitting, and moderate quality of fitting subject to checks, respectively.

	FM set					SFM set				
Model ID	**DS1**	**DS2**	**DS3**	**DS4**	**DS5**	**DS1**	**DS2**	**DS3**	**DS4**	**DS5**
M1a	MQ*	MQ*	MQ*	MQ*	MQ*	HQ*	HQ	HQ*	HQ*	HQ*
M1b	MQ*	MQ*	MQ*	MQ*	MQ*	HQ*	HQ*	HQ*	HQ*	HQ*
M1c	MQ*	MQ*	MQ*	MQ*	MQ*	HQ	HQ	HQ	HQ	HQ*
M1a	MQ*	MQ*	MQ*	MQ*	MQ*	HQ	HQ	HQ	HQ	HQ*
M1b	MQ*	MQ*	MQ*	MQ*	MQ*	HQ	HQ	HQ	HQ	HQ*
M1c	MQ*	MQ*	MQ*	MQ*	MQ*	HQ	HQ	HQ	HQ	HQ
M1a	HQ	HQ	HQ	MQ	MQ*	MQ	HQ	HQ	HQ	HQ
M1b	HQ	HQ	HQ	MQ	MQ	MQ	HQ	HQ	HQ	HQ
M1c	HQ	HQ	HQ	MQ	MQ	HQ	HQ	HQ	HQ*	HQ
M1a	HQ	HQ	HQ	HQ*	HQ	HQ	HQ	HQ*	HQ*	HQ*
M1b	HQ	HQ	MQ*	HQ*	MQ*	HQ	HQ	HQ*	HQ*	HQ*
M1c	HQ	HQ	HQ*	HQ*	HQ*	HQ*	HQ*	HQ*	HQ*	HQ*

TABLE 3 Linear correlations between fragility parameters (median x_M and logarithmic standard deviation σ) and elastic frequency (f_a) for all floor motion (FM), strong floor motion (SFM), far field floor motion (FFFM), and near field floor motions (NFFM) sets and all damage states (DSs), and related coefficient of determination (R^2).

		$x_M = a_{11}\, f_a + a_{12}$			$\sigma = a_{21}\, f_a + a_{22}$		
FM set	**DS**	a_{11}	a_{12}	R^2	a_{21}	a_{22}	R^2
FM	DS1	0.165	0.260	0.802	−0.077	0.844	0.685
	DS2	0.322	0.555	0.794	−0.072	0.813	0.694
	DS3	0.490	0.945	0.831	−0.086	0.794	0.740
	DS4	0.500	1.970	0.736	−0.111	0.899	0.845
	DS5	0.364	3.715	0.510	−0.114	0.997	0.918
SFM	DS1	0.191	0.188	0.766	−0.041	0.529	0.540
	DS2	0.372	0.411	0.756	−0.039	0.517	0.610
	DS3	0.550	0.704	0.822	−0.051	0.492	0.534
	DS4	0.547	1.605	0.793	−0.069	0.587	0.745
	DS5	0.405	3.253	0.584	−0.082	0.722	0.864
FFFM	DS1	0.192	0.137	0.824	−0.059	0.727	0.818
	DS2	0.377	0.308	0.820	−0.054	0.691	0.861
	DS3	0.545	0.659	0.854	−0.060	0.604	0.743
	DS4	0.546	1.541	0.808	−0.076	0.635	0.769
	DS5	0.391	3.198	0.606	−0.073	0.652	0.919
NFFM	DS1	0.137	0.401	0.743	−0.091	0.927	0.510
	DS2	0.264	0.833	0.730	−0.086	0.902	0.502
	DS3	0.433	1.260	0.779	−0.111	0.957	0.673
	DS4	0.449	2.461	0.624	−0.141	1.115	0.829
	DS5	0.333	4.303	0.388	−0.149	1.281	0.903

(MQ*); this occurs in about 55% and null cases for FM and SFM sets, respectively. The summary of the quality of fitting assessment is reported in Table 2.

4.4 | Influence of model frequency on fragility parameters

Figure 12 shows the evolution of median x_M and logarithmic standard deviation σ over the model frequency f_a, respectively, considering FM sets; f_a is reported in logarithmic scale since lower frequencies are associated with more models than higher ones. The single model results are reported as markers corresponding to relevant f_a, and best-fitting curves are also depicted. The fragility results associated with the investigated protocols are depicted for all models in Figure 13.

Considering FM sets, the fragility median x_M (Figure 12) overall tends to increase as the frequency f_a grows, even though the different models belonging to the same frequency range are associated with a non-negligible dispersion in terms of x_M, even within elastic response (i.e., considering DS1 and DS2). Nevertheless, clear x_M to f_a linear tendencies are identified (f_a is reported in logarithmic scale). As expected, the results corresponding to DS4 and DS5 are significantly less regular and more dispersed than the ones associated with DS1 to DS3. The quality of fitting related to DS4 and DS5 is expectably significantly lower than the one associated with DS1 to DS3.

Figure 14 shows the coefficient of determination (R^2) associated with the linear fitting lines. R^2 associated with median fitting is significantly high over DS1 to DS3 for all FM sets, for example, ranging from 0.75 to 0.85, whereas, for DS4 and especially DS5, the coefficient tends to decrease, for example, within 0.60–0.80 (0.40–0.60) for DS4 (DS5). Overall, FFFM (NFFM) results are associated with higher (lower) R^2.

Table 3 reports the linear fitting coefficients and related R^2 defining the estimated fragility to elastic frequency correlations. The abovementioned results show that the elastic frequency might be correlated with seismic damage with a moderate efficiency even out of the elastic range, but due consideration is needed to interpret and apply the results, given the relatively lower abovementioned fitting quality. Considering the fitting lines, the influence of the FM set might be significant, depending on DS, frequency range, and specific model. In particular, this influence is lower over medium

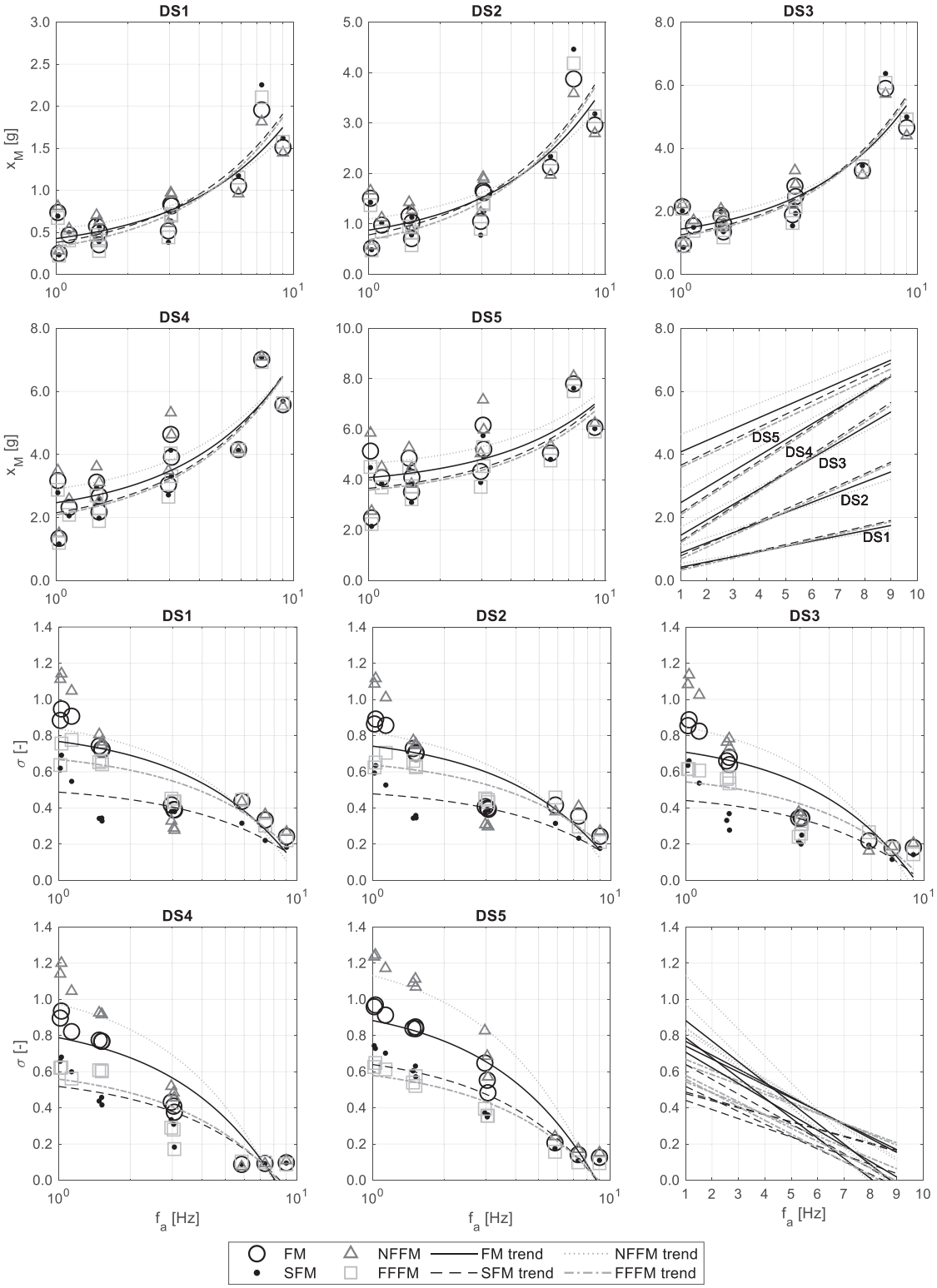

FIGURE 12 Fragility median (x_M) and logarithmic standard deviation (σ) as a function of elastic frequency (f_a) associated with floor motion (FM) sets, evaluated for all damage states (DSs). The response associated with investigated models (depicted by markers) is fitted by linear equations.

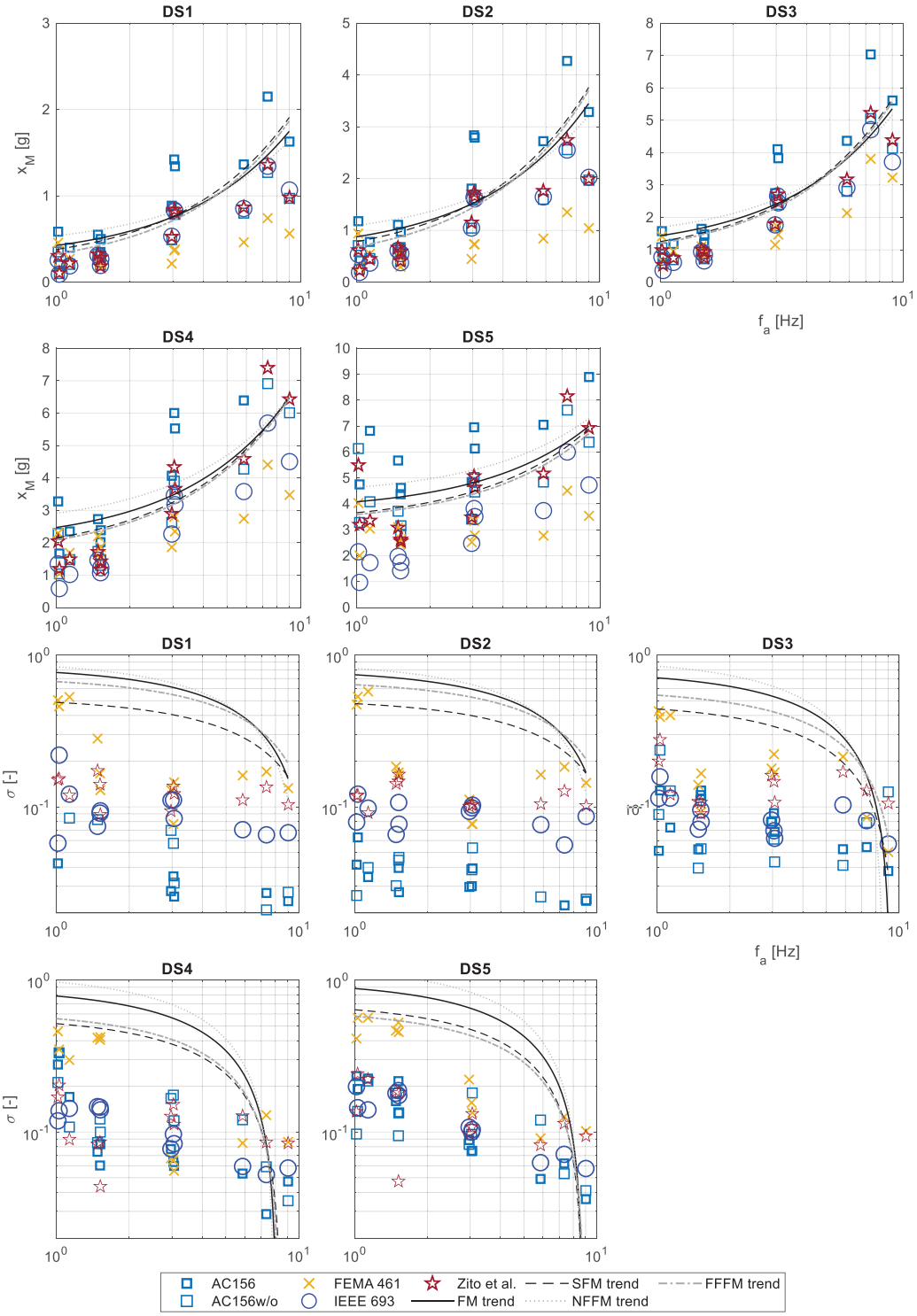

FIGURE 13 Fragility median (x_M) and logarithmic standard deviation (σ) as a function of elastic frequency (f_a) associated with all protocols (single model markers) and floor motion (FM) sets (fitting curves), evaluated for all damage states (DSs).

frequencies for DS1 to DS3, corresponding to which the different FM set curves tend to merge. For DS4 and DS5, the influence of the FM set decreases as f_a grows, but, while all FM set curves tend to converge at the highest frequency for DS4, for DS5, the discrepancy among the curves is still relatively significant over the highest frequencies and the discrepancy reduction is not major. Overall, FFFM and SFM curves are quite similar for all DSs, and the former is slightly more severe, that is, associated with lower x_M. It is worth noting that both intercept and slope of fitting lines increase from DS1 to DS4, whereas only intercept increases passing from DS4 to DS5, and the slope of DS5 curve is more comparable with DS2.

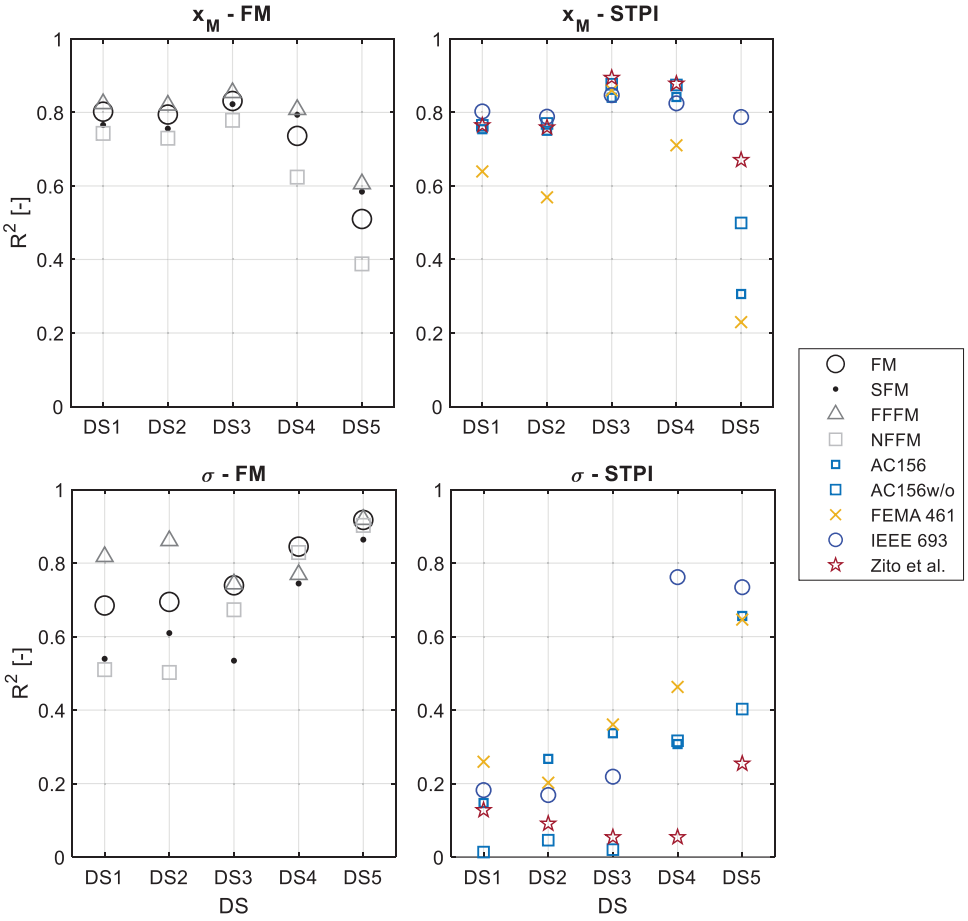

FIGURE 14 Coefficient of determination (R^2) as a function of the investigated damage states (DSs) for floor motion (FM) and shake table protocol input (STPI) sets.

x_M versus f_a curves associated with the investigated DSs are clearly distinct among them and might be considered references for expeditious but relatively reliable estimation of fragility medians, as a function of the elastic frequency of the element. Obviously, these capacities refer to specific SDOF models, even though varying their main geometrical/structural features. In this context, these curves are meant as NE capacity curves or capacity spectra. As a matter of fact, they define a measure of NE capacity associated with several DSs, expressed as a function of elastic frequency. The provided fragility parameters, considering the empirical values or the fitted curves, can be used to estimate statistical capacity thresholds that are more or less conservative than the provided medians, according to the requirements or desired level of safety.

The FM sets have a major influence on logarithmic standard deviation σ (Figure 12), and σ regularly decreases as f_a grows. In particular, the FM set σ curves tend to converge at the highest frequencies for all DSs. A linear pattern of σ is found over f_a, with R^2 that is, in some cases, relatively high, and always greater than 0.5 (Figure 14). An inversion of tendency is observed regarding the influence of DSs on R^2. In particular, σ-based R^2 related to DS4 and DS5 is significantly higher than DS1 to DS3 one, and the former R^2 show a reduced dispersion of the different FM sets. Conversely, σ-based R^2 related to DS1 to DS3 are quite dispersed, and they range within 0.5–0.85 over the different FM sets.

It is worth noting that while the different DSs majorly affect the median x_M an opposite trend is found with regard to the logarithmic standard deviation σ. σ is not particularly affected by the different DSs and does not significantly vary within the model frequency ranges. The fitting curves reported in Figure 12 provide uncertainty measures accounting for several key sources, that is, record to record variability, modeling, elastic frequency. Therefore, they could be usefully implemented to consider these dispersion measures in future studies, even though their robustness should still be validated by more comprehensive analyses.

Figure 13 depicts the evolution of median (x_M) and logarithmic standard deviation (σ) over the model frequency (f_a), respectively, for all protocols (single model results) and FM sets (fitting curves). The comparison between FM and protocol

set fragilities, in terms of x_M and σ (Figure 13) characterizes the capacity of the protocols (and related experimental procedures) as means for the estimation of seismic capacities since FM sets are reasonably representative of realistic demand scenarios. Except for AC156 and very few cases associated with the other protocols, the protocols err on the side of caution regarding fragility medians, and the median safety factor, that is, median FM to median protocol ratio, strongly depends on the investigated DSs and model frequencies.

AC156 often overestimates the seismic capacity, that is, corresponding to (a) medium to large frequencies for DS1 to DS4 and (b) all frequencies for DS5. For DS4, M1a is associated with relatively unsafe capacity estimation. IEEE 693 (FEMA 461) protocol almost always (often) produces conservative estimations, but the associated protocol capacities are extremely conservative in some cases, for example, low frequencies for DS4 and DS5 (medium to high frequencies for DS1 and DS2). Zito et al. protocol is overall associated with reliable but not extremely conservative capacity estimations, and only in few cases it overestimates the capacity, for example, minor overestimation for medium frequencies and DS1 to DS5, and more significant overestimation for model M4b and DS3 to DS5 and model M1a and DS5. AC156 w/o shows fragility medians relatively similar to Zito et al.

In terms of dispersion (Figure 13), all protocols are typically associated with σ lower or significantly lower than FM one, and the trends over f_a are different or significantly different from the ones associated with FM sets (Figure 13). In particular, σ is approximately constant or slightly decreases with f_a over DS1 to DS3, whereas a more significant and regular decreasing trend, still being less significant than FM sets one, is observed considering DS4 and DS5. FEMA 461 protocol supplies dispersion that are more comparable with FM ones for low and high frequencies and over all DSs, whereas the other protocols produce dispersions more comparable with FM ones only for high or very high frequencies, especially over DS4 and DS5. The evidence shows that the protocols have a clear control on the capacity dispersions, that is certainly a positive feature, which strengthens their reliability in case the median estimations are conservative. Further comments on the dispersions of the protocols are omitted since this falls beyond the scope of the study.

The protocol fragility parameters were also assessed in terms of tendency line, and the related R^2 values are shown in Figure 14 for the sake of completeness. However, this fitting is less significant than the one associated with FMs. As a matter of fact, FM fitting can be referred to as an expeditious assessment of seismic capacity under FMs, whereas the fitting related to the protocol sets only has a limited scientific meaning and does not provide applicative tools. It is recalled that the fitting correlations refer to the implemented models and to the reference case studies, and these results should be applied to other cases studies with due consideration. However, it can be noted that a trend similar to the one related to FM is found regarding x_M-based R^2, except for FEMA 461 protocol that shows relatively lower R^2 values. σ-based R^2 related to the protocol sets is overall quite reduced, except for very few cases, that is, (a) IEEE 693 for DS4 and (b) IEEE 693, FEMA 461, and AC156w/o for DS5. Therefore, the fitting correlation cannot be considered significant.

5 | CONCLUSIONS

The study provides a comprehensive assessment of the seismic response and capacity of acceleration-sensitive NEs housed in RC buildings. In particular, NEs are modeled as elastic-plastic (with hardening and softening) SDOF systems, and IDA is carried out. Seismic inputs associated with STPs are also considered as loading histories. The results consist of (a) IDA curves, (b) (acceleration) component amplification factors (CAFs), and fragility curves. In particular, the influence of the model frequency on the fragility parameters is assessed. The remarks of the study are identified in the following.

(1) CAF overall decreases as PFA grows, as expectable, according to the evolution from the elastic to the inelastic behavior. In particular, lower frequency NEs are associated with more regular tendencies, and the highest (elastic) CAF might be greater than 2.5–3, depending on the specific frequency or model characteristics, whereas CAF associated with heavily plastic response tends to the unity, or in some cases (e.g., extremely high-frequency models), might even be lower. Elastic-based CAF estimations reflect the elastic properties of the modeled SDOF and might be generalized considering the provide stiffnes-mass combinations and/or fundamental SDOF frequencies. The uncertainty influence mostly associated with record-to-record and less to the model characteristics tends to be lower (higher) for low (high) frequency models.
(2) STPs tend to supply relatively safe or extremely overconservative CAF values, if compared with reference FM responses, even though, in few cases, the protocols might underestimate CAF. The study provides useful CAF thresholds associated with the elastic response due to representative sets of real building floor motions, essential for an accurate seismic demand estimation.

(3) Fragility medians are overall well correlated to the elastic frequency of the models through linear trends, even considering DSs associated with the inelastic response. The fragility dispersion tends to decrease as the elastic frequency grows, also over inelastic DSs. Linear trends might also be associated with the fragility dispersion over the abovementioned parameter, even though the coefficient of determination might not be always adequately high. The coefficients of determination associated with the median estimations are overall good (very few cases with values lower than 0.6), whereas the correlations related to the dispersion estimations are less efficient in terms of coefficient of determination. Fragility correlation equations and related coefficients of determinations are provided in the study, and these measures might be useful for expeditious capacity assessment of NEs compatible with case study ones. The readers are recommended to refer to the provided efficiency measures (quality of fitting and coefficient of determination) prior to applying the provided closed-form equations.
(4) STPs, except AC156, tend to provide safe or excessively conservative median estimations if compared with reference FMs, even though in very few cases (neglecting AC156), the estimations can be slightly unsafe. As expectable, the fragility dispersion associated with the investigated protocols is overall lower or significantly lower than the one related to the reference FM set, and a more comparable dispersion is only generally found for FEMA 461 and, for all protocols, over high-frequency models.

The study sheds light on the seismic response of acceleration-sensitive building NEs and provides quantitative response and capacity measures, useful for expeditious assessment of NEs that are compatible with the case study models. Whereas the methodological framework is general and wide applicable, the quantitative measures of capacity, referring to the empirical fragilities and the fitting correlations, should be used with due consideration, considering the compatibility with the implemented methods and investigated case studies. The provided empirical or fitted uncertainty measures could be considered in order to supply more or less conservative capacity measures, assuming a lognormal model and setting the provided median values. Further studies should be carried out by extending the methodology to different case study NEs, possibly considering other building types, for example, steel structures. Finally, the provided correlations should be experimentally validated by implementing dynamic tests and assessing statistical-based response and capacity measures.

ACKNOWLEDGMENTS

The study was mostly funded by (1) the Italian Ministry of University and Research (MUR) in the framework of PRIN 2020 project titled "ENRICH project: ENhancing the Resilience of Italian healthCare and Hospital facilities" and minorly by (2) the Italian Department of Civil Protection (DPC) in the framework of the National project DPC—ReLUIS 2022–2024 WP17: "Code contributions for nonstructural elements"). Dr. Martino Zito is thanked for the technical support regarding the data elaboration.

CONFLICT OF INTEREST STATEMENT

The authors declare no conflicts of interest.

DATA AVAILABILITY STATEMENT

The data presented in the paper, including the fragility estimates and fitting curves, are available from the corresponding author, GM, upon reasonable request.

ORCID

Gennaro Magliulo https://orcid.org/0000-0002-1812-4357
Danilo D'Angela https://orcid.org/0000-0002-8096-5202

REFERENCES

1. Deierlein GG, Krawinkler H, Cornell CA, A framework for performance-based earthquake engineering. 2003.
2. FEMA. *FEMA P-58-3: Seismic Performance Assessment of Buildings. Performance Assessment Calculation Tool (PACT)*. 2012.
3. Perrone D, Calvi PM, Nascimbene R, Fischer EC, Magliulo G. Seismic performance of non-structural elements during the 2016 Central Italy earthquake. *Bull Earthquake Eng*. 2019;17(10):5655-5677. doi:10.1007/s10518-018-0361-5
4. Arifin FA, Sullivan TJ, MacRae G, Kurata M, Takeda T. Lessons for loss assessment from the Canterbury earthquakes: a 22-storey building. *Bull Earthquake Eng*. 2021;19(5):2081-2104. doi:10.1007/s10518-021-01055-7
5. Achour N, Miyajima M, Kitaura M, Price A. Earthquake-induced structural and nonstructural damage in hospitals. *Earthq Spectra*. 2011;27(3):617-634. doi:10.1193/1.3604815

6. Bianchi S, Ciurlanti J, Perrone D, et al. Shake-table tests of innovative drift sensitive nonstructural elements in a low-damage structural system. *Earthq Eng Struct Dyn*. 2021;50(9):2398-2420. doi:10.1002/eqe.3452
7. Porter K, Kennedy R, Bachman R. Creating fragility functions for performance-based earthquake engineering. *Earthq Spectra*. 2007;23(2):471-489. doi:10.1193/1.2720892
8. Guzman Pujols JC, Ryan KL. Development of generalized fragility functions for seismically induced content disruption. *Earthq Spectra*. 2016;32:1303-1324. doi:10.1193/081814EQS130M
9. Zito M, Nascimbene R, Dubini P, D'Angela D, Magliulo G. Experimental seismic assessment of nonstructural elements: testing protocols and novel perspectives. *Buildings*. 2022;12(11):1871. doi:10.3390/buildings12111871
10. Magliulo G, Pentangelo V, Maddaloni G, et al. Shake table tests for seismic assessment of suspended continuous ceilings. *Bull Earthquake Eng*. 2012;10(6):1819-1832. doi:10.1007/s10518-012-9383-6
11. Ghith A, Ezzeldin M, Tait M, El-Dakhakhni W. Shake table seismic performance assessment of auxiliary battery power systems using the FEMA 461 protocol. *J Struct Eng*. 2019;145(8):04019080. doi:10.1061/(ASCE)ST.1943-541X.0002341
12. Wittich CE, Hutchinson TC. Shake table tests of stiff, unattached, asymmetric structures: shake table tests of stiff, unattached, asymmetric structures. *Earthq Eng Struct Dyn*. 2015;44(14):2425-2443. doi:10.1002/eqe.2589
13. Soroushian S, Maragakis E, "Manos" Ryan KL, et al. Seismic simulation of an integrated ceiling-partition wall-piping system at e-defense. ii: evaluation of nonstructural damage and fragilities. *J Struct Eng*. 2016;142(2):04015131. doi:10.1061/(ASCE)ST.1943-541X.0001385
14. Guzman J, Ryan KL. Data from the network for earthquake engineering simulation/e-defense collaborative test program on innovative isolation systems and nonstructural components. *Earthq Spectra*. 2015;31(2):1195-1209. doi:10.1193/083113EQS241
15. Mazza F. In-plane–out-of-plane non-linear model of masonry infills in the seismic analysis of r.c.-framed buildings. *Earthq Eng Struct Dyn*. 2018;48(4):432-453. doi:10.1002/eqe.3143. eqe.3143.
16. Rezvani R, Soroushian S, Zaghi AE, Maragakis M. Numerical seismic fragility analysis for suspended ceilings with various geometries. *J Build Eng*. 2022;54:104627. doi:10.1016/j.jobe.2022.104627
17. Belghiat C, Plassiard JP, Messabhia A, Plé O, Guenfoud M. Analytical and numerical study of double-panel confined masonry walls. *J Build Eng*. 2021;39:102322. doi:10.1016/j.jobe.2021.102322
18. Petrone C, Coppola O, Magliulo G, Lopez P, Manfredi G. Numerical model for the in-plane seismic capacity evaluation of tall plasterboard internal partitions. *Thin Walled Struct*. 2018;122:572-584. doi:10.1016/j.tws.2017.10.047
19. Brandolese S, Fiorin L, Scotta R. Seismic demand and capacity assessment of suspended ceiling systems. *Eng Struct*. 2019;193:219-237. doi:10.1016/j.engstruct.2019.05.034
20. Jiang H, Wang Y, Huang Y. Shaking table tests and numerical modeling of discontinuous suspended ceiling system with free boundary condition. *Eng Struct*. 2022;273:115069. doi:10.1016/j.engstruct.2022.115069
21. D'Angela D, Magliulo G, Cosenza E. Seismic damage assessment of unanchored nonstructural components taking into account the building response. *Struct Saf*. 2021;93:102126. doi:10.1016/j.strusafe.2021.102126
22. Vitanova M, Bogdanovic A, Bozinovski Z, et al. Seismic performance validation for RC building structures damaged by Durres earthquake, Mw6.4, 26 November 2019, Albania. *Bull Earthquake Eng*. 2022;20(12):6527-6554. doi:10.1007/s10518-022-01453-5
23. Derakhshan H, Walsh KQ, Ingham JM, Griffith MC, Thambiratnam DP. Seismic fragility assessment of nonstructural components in unreinforced clay brick masonry buildings. *Earthq Eng Struct Dyn*. 2020;49(3):285-300. doi:10.1002/eqe.3238
24. Feinstein T, Moehle JP. Seismic response of floor-anchored nonstructural components fastened with yielding elements. *Earthq Eng Struct Dyn*. 2022;51(1):3-21. doi:10.1002/eqe.3553
25. Feinstein T, Moehle JP. Mechanics based numerical modeling of floor-anchored nonstructural components. *J Struct Eng*. 2023;149(1):04022213. doi:10.1061/(ASCE)ST.1943-541X.0003496
26. Kazantzi AK, Miranda E, Vamvatsikos D. Strength-reduction factors for the design of light nonstructural elements in buildings. *Earthq Eng Struct Dyn*. 2020;49(13):1329-1343. doi:10.1002/eqe.3292
27. Obando JC, Lopez-Garcia D. Inelastic displacement ratios for nonstructural components subjected to floor accelerations. *J Earthquake Eng*. 2018;22(4):569-594. doi:10.1080/13632469.2016.1244131
28. Cremen G, Baker JW. Improving FEMA P-58 non-structural component fragility functions and loss predictions. *Bull Earthquake Eng*. 2019;17(4):1941-1960. doi:10.1007/s10518-018-00535-7
29. Vukobratović V, Fajfar P. A method for the direct estimation of floor acceleration spectra for elastic and inelastic MDOF structures. *Earthq Eng Struct Dyn*. 2016;45(15):2495-2511. doi:10.1002/eqe.2779
30. Petrone C, Magliulo G, Manfredi G. Seismic demand on light acceleration-sensitive nonstructural components in European reinforced concrete buildings. *Earthq Eng Struct Dyn*. 2015;44(8):1203-1217. doi:10.1002/eqe.2508
31. Anajafi H, Medina RA, Santini-Bell E. Inelastic floor spectra for designing anchored acceleration-sensitive nonstructural components. *Bull Earthquake Eng*. 2020;18(5):2115-2147. doi:10.1007/s10518-019-00760-8
32. Kazantzi AK, Vamvatsikos D, Miranda E. Evaluation of seismic acceleration demands on building nonstructural elements. *J Struct Eng*. 2020;146(7):04020118. doi:10.1061/(ASCE)ST.1943-541X.0002676
33. Qi L, Kunitomo K, Kurata M, Ikeda Y. Investigating the vibration properties of integrated ceiling systems considering interactions with surrounding equipment. *Earthq Eng Struct Dyn*. 2020;49(8):772-793. doi:10.1002/eqe.3264
34. Petrone C, Magliulo G, Manfredi G. Floor response spectra in RC frame structures designed according to Eurocode 8. *Bull Earthquake Eng*. 2016;14(3):747-767. doi:10.1007/s10518-015-9846-7

35. American Society of Civil Engineers. *Minimum design loads and associated criteria for buildings and other structures*. 7th ed. American Society of Civil Engineers; 2021. doi:10.1061/9780784415788
36. British Standards Institution, European committee for standardization. *Eurocode 8, design of structures for earthquake resistance*. British Standards Institution; 2005.
37. Ministero delle Infrastrutture e dei Trasporti. D.M. del 17/01/2018 – "Aggiornamento delle Norme tecniche per le Costruzioni 2018" NTC 2018 (in Italian) 2018.
38. Flores FX, Lopez-Garcia D, Charney FA. Assessment of floor accelerations in special steel moment frames. *J Constr Steel Res*. 2015;106:154-165. doi:10.1016/j.jcsr.2014.12.006
39. Villaverde R. Simple method to estimate the seismic nonlinear response of nonstructural components in buildings. *Eng Struct*. 2006;28(8):1209-1221. doi:10.1016/j.engstruct.2005.11.016
40. Sullivan TJ, Calvi PM, Nascimbene R. Towards improved floor spectra estimates for seismic design. *Earthq Struct*. 2013;4(1):109-132. doi:10.12989/EAS.2013.4.1.109
41. McKenna F, Fenves GL, Scott MH. OpenSees: open system for earthquake engineering simulation. *Pacific Earthquake Engineering Research Center*. University of California,Berkeley. http://opensees.berkeley.edu. Available at: 2000.
42. Ibarra LF, Medina RA, Krawinkler H. Hysteretic models that incorporate strength and stiffness deterioration. *Earthq Eng Struct Dyn*. 2005;34(12):1489-1511. doi:10.1002/eqe.495
43. Ibarra LF, Krawinkler H. *Global collapse of frame structures under seismic excitations*. The John A. Blume Earthquake Engineering Center. Department of Civil and Environmental engineering. Stanford University; 2005.
44. Lignos DG, Krawinkler H. Development and utilization of structural component databases for performance-based earthquake engineering. *J Struct Eng*. 2013;139(8):1382-1394. doi:10.1061/(ASCE)ST.1943-541X.0000646
45. Lignos DG, Krawinkler H. Deterioration modeling of steel components in support of collapse prediction of steel moment frames under earthquake loading. *J Struct Eng*. 2011;137(11):1291-1302. doi:10.1061/(ASCE)ST.1943-541X.0000376
46. Lignos DG, Krawinkler H, A steel database for component deterioration of tubular hollow square steel columns under varying axial load for collapse assessment of steel structures under earthquakes. *Proceedings of the 7th International Conference on Urban Earthquake Engineering (7CUEE) & 5th International Conference on Earthquake Engineering (5ICEE)*, Tokyo, Japan: 2010.
47. D'Angela D, Magliulo G, Cosenza E. Characterization of local and global capacity criteria for collapse assessment of code-conforming RC buildings. *Bull Earthquake Eng*. 2021;19:3701-3743. doi:10.1007/s10518-021-01115-y
48. Ricci P, Manfredi V, Noto F, et al. Modeling and seismic response analysis of italian code-conforming reinforced concrete buildings. *J Earthquake Eng*. 2018;22(sup2):105-139. doi:10.1080/13632469.2018.1527733
49. Haselton CB, Deierlein GG. *Assessing seismic collapse safety of modern reinforced concrete moment frame buildings*. The John A. Blume Earthquake Engineering Center. Department of Civil and Environmental engineering. Stanford University; 2007.
50. Kecman D. Bending collapse of rectangular and square section tubes. *Int J Mech Sci*. 1983;25(9–10):623-636. doi:10.1016/0020-7403(83)90072-3
51. Charney FA. Unintended consequences of modeling damping in structures. *J Struct Eng*. 2008;134(4):581-592. doi:10.1061/(ASCE)0733-9445(2008)134:4(581)
52. Vamvatsikos D, Cornell CA. Incremental dynamic analysis. *Earthq Eng Struct Dyn*. 2002;31(3):491-514. doi:10.1002/eqe.141
53. CESMD. Center for Engineering Strong Motion Data 2017. Download on October 31st 2017. www.strongmotioncenter.org
54. Mosleh A, Razzaghi MS, Jara J, Varum H. Seismic fragility analysis of typical pre-1990 bridges due to near- and far-field ground motions. *Int J Adv Struct Eng*. 2016;8(1):1-9. doi:10.1007/s40091-016-0108-y
55. Fragiadakis M, Diamantopoulos S. Fragility and risk assessment of freestanding building contents. *Earthq Eng Struct Dyn*. 2020;49(10):1028-1048. doi:10.1002/eqe.3276
56. Zou X, Yang W, Liu P, Wang M. Floor acceleration amplification and response spectra of reinforced concrete frame structure based on shaking table tests and numerical study. *Arch Civ Mech Eng*. 2023;23(3):156. doi:10.1007/s43452-023-00648-0
57. International Code Council Evaluation Service (ICC-ES). *AC156 acceptance criteria for the seismic qualification of nonstructural components*. 2012.
58. Federal Emergency Management Agency (FEMA). *Interim protocols for determining seismic performance characteristics of structural and nonstructural components through laboratory testing*. Report No. FEMA 461. 2007.
59. Institute of Electrical and Electronics Engineers. *693–2006 IEEE Recommended practice for seismic design for substations*. Institute of Electrical and Electronics Engineers; 2006.
60. Zito M, D'Angela D, Maddaloni G, Magliulo G. A shake table protocol for seismic assessment and qualification of acceleration-sensitive nonstructural elements. *Comput-Aided Civ Infrastruct Eng*. 2022;38:1699-1726. doi:10.1111/mice.12951. mice.12951.
61. D'Angela D, Magliulo G, Cosenza E. Towards a reliable seismic assessment of rocking components. *Eng Struct*. 2021;230:111673. doi:10.1016/j.engstruct.2020.111673
62. Perrone D, Brunesi E, Decarro F, Peloso S, Filiatrault A, Seismic assessment and qualification of non-structural elements in Europe: a critical review. 4th International Workshop on the Seismic Performance of Non-Structural Elements (SPONSE), Pavia, Italy: 2019. doi:10.7414/4sponse.ID.10
63. Takhirov SM, Fujisaki E, Power B, Vancouver A, Riley WM, Low B. *Development of Time Histories for IEEE693 Testing and Analysis (Including Seismically Isolated Equipment)*. Pacific Earthquake Engineering Research Center, University of California; 2017. PEER Report No. 2017/10.

64. Wilcoski J, Gambill J, Smith S. *CERL equipment fragility and protection procedure (CEFAPP)*. 1997. *USACERL Technical Rep. No. 97/58*.
65. Petrone C, Magliulo G, Manfredi G. Shake table tests on standard and innovative temporary partition walls. *Earthq Eng Struct Dyn*. 2017;46(10):1599-1624. doi:10.1002/eqe.2872
66. Porter K, A beginner's guide to fragility, vulnerability, and risk. 2019.
67. Porter K, Kennedy R, Bachman R. *Developing fragility functions for building components for ATC-58. A Report to ATC-58*. Applied Technology Council, Redwood City; 2006.
68. Lilliefors HW. On the Kolmogorov-Smirnov test for normality with mean and variance unknown. *J Am Statist Assoc*. 1967;62(318):399. doi:10.2307/2283970
69. D'Angela A, Magliulo G, Cosenza E. Incremental dynamic analysis of rigid blocks subjected to ground and floor motions and shake table protocol inputs. *Bull N Z Soc Earthq Eng*. 2022;55(Early access). https://www.bulletin.nzsee.org.nz/index.php/bnzsee
70. Anajafi H, Medina RA. Evaluation of ASCE 7 equations for designing acceleration-sensitive nonstructural components using data from instrumented buildings. *Earthq Eng Struct Dyn*. 2018;47(4):1075-1094. doi:10.1002/eqe.3006
71. Perrone D, Filiatrault A, Peloso S, Brunesi E, Beiter C, Piccinin R. Experimental seismic response evaluation of suspended piping restraint installations. *Bull Earthquake Eng*. 2020;18(4):1499-1524. doi:10.1007/s10518-019-00755-5
72. Bravo-Haro MA, Virreira JR, Elghazouli AY. Inelastic displacement ratios for non-structural components in steel framed structures under forward-directivity near-fault strong-ground motion. *Bull Earthquake Eng*. 2021;19(5):2185-2211. doi:10.1007/s10518-021-01059-3
73. Rodriguez D, Perrone D, Filiatrault A. Seismic demand on non-structural elements for quantifying seismic performance factors. *Earthq Eng Struct Dyn*. 2022;52:1016-1039. doi:10.1002/eqe.3799. eqe.3799.
74. American Society of Civil Engineers. *Minimum design loads and associated criteria for buildings and other structures*. 7th ed. American Society of Civil Engineers; 2017. doi:10.1061/9780784414248
75. New Zealand Society for Earthquake Engineering (NZSEE), Structural Engineering Society (SESOC), NZ Geotechnical Society (NZGS), Innovation and Employment (MBIE), Earthquake Commission (EQC). *The Seismic Assessment of Existing Buildings: Technical Guidelines for Engineering Assessments (the Guidelines)*. 2017.
76. Standards New Zealand. *NZS 1170.5:2004: Structural design actions, Part 5: Earthquake actions*. 2016.
77. Ministero delle Infrastrutture e dei Trasporti. Circolare 21 gennaio 2019, n. 7 C.S.LL.PP. Istruzioni per l'applicazione dell'«Aggiornamento delle "Norme tecniche per le costruzioni"» di cui al decreto ministeriale 17 gennaio 2018. 2019.

How to cite this article: Magliulo G, D'Angela D. Seismic response and capacity of inelastic acceleration-sensitive nonstructural elements subjected to building floor motions. *Earthquake Engng Struct Dyn*. 2024;1-25. https://doi.org/10.1002/eqe.4080